Directed remodeling of the mouse gut microbiome inhibits the development of atherosclerosis

Poshen B. Chen[1], **Audrey S. Black**[1], **Adam L. Sobel**[1], **Yannan Zhao**[1], **Purba Mukherjee**[1], **Bhuvan Molparia**[2,3], **Nina E. Moore**[1], **German R. Aleman Muench**[4], **Jiejun Wu**[4], **Weixuan Chen**[4], **Antonio F. M. Pinto**[5], **Bruce E. Maryanoff**[1], **Alan Saghatelian**[5], **Pejman Soroosh**[4], **Ali Torkamani**[2,3], **Luke J. Leman**[1,*], **M. Reza Ghadiri**[1,6,*]

[1]Department of Chemistry, Scripps Research, La Jolla, California, USA

[2]Department of Integrative Structural and Computational Biology, Scripps Research, La Jolla, California, USA

[3]The Scripps Translational Science Institute, Scripps Research, La Jolla, California, USA

[4]Janssen Research & Development, LLC, San Diego, California, USA

[5]Salk Institute for Biological Studies, La Jolla, California, USA

[6]The Skaggs Institute of Chemical Biology, Scripps Research, La Jolla, California, USA

Abstract

The gut microbiome is a malleable microbial community that can remodel in response to a number of factors, including diet, and contribute to the development of several chronic diseases, including atherosclerosis. We devised an *in vitro* screening protocol of the mouse gut microbiome to discover molecules that can selectively modify bacterial growth. This approach was used to identify cyclic D,L-α-peptides that remodeled the Western diet (WD) gut microbiome toward the low fat diet microbiome state. Daily oral administration of the peptides in WD-fed *LDLr*$^{-/-}$ mice reduced plasma total cholesterol levels and atherosclerotic plaques. Depletion of the microbiome with antibiotics abrogated these effects. Peptide treatment reprogrammed the microbiome transcriptome, suppressed the production of pro-inflammatory cytokines (including IL-6, TNF-α, and IL-1β), rebalanced levels of short-chain fatty acids and bile acids, improved gut barrier integrity, and increased intestinal T regulatory cells. Directed chemical manipulation provides an additional tool to decipher the chemical biology of the gut microbiome and may advance microbiome-targeted therapeutics.

The gut microbiome plays a fundamental role in host physiology and health[1–3]. In humans and animals, gut microbiome dysbiosis can promote onset and progression of chronic diseases, such as cardiovascular disease[3], obesity[4,5], diabetes[6,7], and central nervous system disorders[8]. Diet can play an important role in disease, both by shaping the microbiome and direct effects on the host. For example, consumption of the calorically rich Western diet (WD) can transform the gut microbiome into a maladaptive state, promoting systemic inflammation and progression of chronic diseases, including atherosclerosis[9–11]. Certain gut bacteria convert choline-rich food to trimethylamine (TMA), ultimately leading to increased risk of cardiovascular disease[3]. Other gut bacterial metabolites, such as short-chain fatty acids (SCFA)[12–14], 4-ethylphenylsulfate (4EPS)[15], aromatic amino acid metabolites[16], and secondary bile acids[17–19] also affect host physiology.

Presently, there are three main approaches that have shown some promise in harnessing the therapeutic potential of the gut microbiome[20]. The first uses small molecules to modulate key pathways in gut bacteria (proteins, enzymes, receptors, etc.) that affect disease-relevant metabolites and/or signaling molecules[21–23]. For example, Hazen and coworkers showed that inhibition of gut microbial lyase activity in the TMA production pathway attenuated the development of atherosclerosis *in vivo*[21]. The second approach is that of prebiotics, which aims to remodel the gut microbiota by providing fiber or complex oligosaccharides that promote the growth of certain taxa[24]. While fiber therapy might be generally beneficial and, in some cases, prevent disease progression, it does not constitute a purposeful and directed remodeling of a given microbiota state into another designated state. Probiotics constitute the third main approach, which seeks to beneficially remodel the microbiome by administering live bacteria into the gut. However, there are considerable challenges with probiotics, including potential safety issues and the obstacle of successful engraftment of the administered strain(s), although innovative advances may support engraftment of probiotics[25].

Directed remodeling is an alternative approach for exploring the therapeutic potential of the gut microbiome. We define directed remodeling of the gut microbiome as a process that can alter, in a deliberate and predetermined fashion, the bacterial composition and/or its transcriptome from a given state into another. Given the sensitivity (plasticity) of microbiota to changes in the chemical milieu within the gut, a wide range of compounds, including natural product supplements[26] or prescribed therapeutics[27], have the potential to cause remodeling of the gut microbiota. We postulated that a rational molecular approach for directed microbiome remodeling would require two basic elements: *i)* molecular scaffolds that can potentially exert differential bacterial growth modulating activities against selected members of the gut microbiota, and *ii)* a predictive *in vitro* screen for compound selection for the *in vivo* studies. Here, we report the rationale, approaches, and evidence that synthetic self-assembling cyclic D,L-α-peptides selected from an *in vitro en masse* gut microbiota screen selectively remodel a WD-induced gut microbiome *in vivo* into a low fat diet-like state to prevent the development of atherosclerosis.

Results

A two-state gut microbiome model

Low-density lipoprotein receptor null ($LDLr^{-/-}$) mice have a human-like lipoprotein profile and have been widely used as an animal model for diet-induced atherosclerosis. $LDLr^{-/-}$ mice develop hypercholesterolemia and arterial plaques after several weeks on a WD, but not on a Chow diet (CHD). Feeding a WD to $LDLr^{-/-}$ mice for two weeks caused remodeling of their gut microbiome as compared to mice fed a CHD (Extended Data Fig. 1a, Supplementary Table 1), consistent with the observed impacts of a WD on the gut microbiome of wild-type mice[11]. Thus, depending on the diet, $LDLr^{-/-}$ mice exhibit two distinct gut microbiome states that are associated with different phenotypic outcomes (designated here as: "WD state" exhibiting hyperlipidemia and atherosclerosis phenotype, and "CHD state" exhibiting healthy phenotype). We hypothesized that if the WD-induced gut microbiome is causal in the onset and progression of atherosclerosis in $LDLr^{-/-}$ mice, then remodeling the composition of microbiota *in vivo* (even under the influence of WD) toward a CHD state should ameliorate disease progression, thereby testing the therapeutic potential of gut microbiome remodeling.

Self-assembling cyclic D,L-α-peptides as synthetic bacterial growth modulators.

—Cyclic peptides with an even number of alternating D-, and L-α–amino acid configuration (typically 6 or 8 residues) can self-assemble under conditions that favor hydrogen bonding (such as in a lipid membrane environment) into extended β-sheet-like hollow tubular structures (Fig. 1a)[28–30]. By appropriate choice of the sequence, cyclic D,L-α-peptides can selectively partition into bacterial membranes, interrupt transmembrane potential and/or ion gradients, and impair cell growth[31–33]. We hypothesized that oral administration of a given cyclic D,L-α-peptide sequence, selected to possess differential bacterial growth modulating activities against certain members of the gut microbiota, could be used to remodel the microbiome.

We developed an *en masse* screening approach for assessing the effects of compounds on the gut microbiota as a whole (Fig. 1b). Such an approach would be inherently data rich, internally consistent, and could account for potential indirect growth-modulating effects that might exist within the bacterial community.

En masse in vitro screen

We isolated fresh gut microbiome content from $LDLr^{-/-}$ mice conditioned for at least two weeks on WD by surgically removing cecum under anaerobic conditions. The cecal contents were then mixed with growth media, distributed in 96-well plates, and incubated overnight in the presence of the test peptides. The activity and selectivity of each peptide for remodeling the gut microbiota community was assessed *en masse* by 16S rRNA sequencing of each well. A number of challenges had to be addressed in developing this protocol, including inoculum handling, choice of growth media, assay duration, etc. Our current assay culture condition maintains 50 bacterial genera (overnight culture), which is fairly representative of the 67 genera found in the uncultured community (Supplementary Table 2). As expected, the overnight in vitro culturing resulted in changes in the relative composition

of the microbiome (Extended Data Fig. 2), but the assay condition maintains a sufficient bacterial diversity to enable *en masse* assessment of the relative changes in bacterial composition between peptide-treated and untreated samples.

Our laboratory maintains a library of approximately 1,500 diverse cyclic D,L-α-peptide sequences (pure and spectroscopically characterized) that possess a range of antimicrobial activity and species selectivity determined from previous studies[35,36]. For the present study we selected 29 cyclic D,L-α-peptides from this library of antimicrobial peptides based on sequence diversity and lack of mammalian cell toxicity (Fig. 1c, Supplementary Table 3). We observed a range of microbiota remodeling effects in the *en masse* screen, largely without diminishing microbiota alpha diversity (the number and evenness of bacterial taxa within the community) (Extended Data Fig. 1b). Sixteen of the peptides substantially increased the Bacteroidetes/Firmicutes ratio[34] in the culture, while three peptides decreased the ratio (Extended Data Fig. 1c). From a pairwise comparison of the activities of the different cyclic peptides, we found six distinct peptide clusters, each of which affected the microbiota differently from the other clusters (Fig. 1d). To further support that the peptides directly affect bacterial growth in culture, we performed a series of *in vitro* MIC assays against nine representative laboratory strains of gut bacteria, and we carried out *in vitro en masse* screening with several control peptides (mode of action probes) (Extended Data Fig. 3). The control peptides are stereoisomers (enantiomers and diastereomers) or *N*-methylated analogs of peptides **1** and **11** (Extended Data Fig. 4). Whereas peptides **1** and **11** did remodel the microbiota community in vitro and exhibited antibacterial activity in the MIC assays, the control peptides did not affect bacterial growth (Extended Data Fig. 3), despite having the identical amino acid sequences of **1** and **11**. These results are consistent with the expected mechanism of bacterial growth modulation being dependent on peptide self-assembly and bacterial membrane activity. I*n vitro* microbiome remodeling performed in triplicate for peptides **1** and **11** indicated good reproducibility (Extended Data Fig. 3).

We used a distance scoring algorithm for a more refined compound selection, in which peptides that remodel the microbiota community most completely from the WD state toward the CHD state are scored higher (Extended Data Fig. 1d). Briefly, we first eliminated cyclic D,L-α-peptides that had broad-spectrum antibacterial activity (inhibit 95% of growth of 20 species in the community). The remaining compounds were then ranked based on how well they suppressed the bacterial species that grew in abundance in WD-fed mice compared to CHD-fed mice (see Supplementary Table 4 for peptide ranking). Based on these analyses, we chose two peptides for further *in vivo* validation and efficacy studies: the cationic peptide **1**, c[wLwKhShK], and the zwitterionic peptide **11**, c[wLwReQeR], which ranked high within their respective peptide clusters (Figure 1d).

***In vivo* directed remodeling of the gut microbiome.**—We carried out a 10-week study of cyclic peptides c[wLwKhShK] and c[wLwReQeR] vs. vehicle-treated WD and CHD controls in *LDLr*^{−/−} mice to determine the safety and effects of the peptides on the gut microbiota and on atherosclerosis. The abiotic structures of cyclic D,L-α-peptides renders them proteolytically stable, allowing oral administration (*ad libitum* in the drinking water, ~35 mg/kg/day peptide dose). There were no signs of discomfort or toxicity (body weight, liver and spleen weight, AST and ALT enzyme levels), even after a 10-week daily-dosing

regimen (Extended Data Fig. 5). Pharmacokinetic and excretion studies involving c[wLwKhShK] and c[wLwReQeR] demonstrated that these peptides are non-absorbable (lack oral systemic bioavailability), remain largely intact throughout the gut, and are cleared via fecal excretion (Supplementary Table 5, Extended Data Fig. 6), thereby strongly supporting the gut as the site of action.

As predicted from the *in vitro* screen, the Bacteroidetes/Firmicutes ratio[34] increased (within 2 weeks by peptide c[wLwKhShK] and within 6 weeks by peptide c[wLwReQeR]) in treated animals relative to the vehicle WD-fed group (Fig. 2a and Extended Data Fig. 7). Consistent with previous reports[11,35,36], we also observed reduction in gut microbiome richness (Chao1 index) in WD-fed *LDLr*^{−/−} mice, but administration of peptides **1** and **11** to the WD-fed mice reversed this reduction in gut microbiome richness, restoring it to a level similar to that of CHD-fed mice (Extended Data Fig. 7). Consistent with the *in vitro* screen (Fig. 1c), zwitterionic peptide c[wLwReQeR] acted more selectively *in vivo* against WD-remodeled gut bacteria than the cationic peptide c[wLwKhShK] (Fig. 2b and Extended Data Fig. 8). The two peptides initially targeted different bacterial genera but over the course of the 10-week study, the remodeled gut microbiome induced by the peptides became more similar (Extended Data Fig. 7). Although the overall microbiota alpha diversity was unchanged by peptide treatment (Fig. 2c), the microbiota populations in treated animals were distinct from untreated animals (Fig. 2d). A total of 73 OTUs were identified at the species level in the culture of the in vitro assay; similarly, 72 OTUs were identified at the species level in the uncultured mouse cecum samples. Of these, 42 species (~58%) were present in both the cultured and uncultured samples. Out of these 42 species, 14 species underwent statistically significant changes in abundance after peptide treatment in vivo, while the other 28 species remained unaffected by peptide treatment. Of the 14 species that were significantly affected by peptide treatment in vivo, most were affected in the same general way in the *in vitro* assay (Fig. 2e), supporting that the assay can be predictive of changes *in vivo*.

Transcriptional reprogramming of gut microbiota and metabolic effects.

Peptide treatment induced widespread reprogramming of the microbiota transcriptome, as determined by RNA-Seq of bacterial RNA from the feces following a 2-week treatment period (Fig. 3a). The observed gene expression differences (out of ~53,800 total annotated bacterial genes) could be grouped into three main clusters. Two clusters contained bacterial genes for which expression was increased (Cluster 1) or decreased (Cluster 2) by peptide treatment. Cluster 3 contained genes that were altered by the WD, but not affected by peptide treatment. The majority of bacterial species in the feces sample contained genes present in all three clusters (Fig. 3), indicative of pervasive changes not only to the structure, but also the transcriptional activities of the microbiota. Overall gene expression from Firmicutes was reduced and overall gene expression from Bacteroidetes was increased by c[wLwReQeR] treatment (Clusters 1 compared to Cluster 2 and 3) (Extended Data Fig. 9).

At the metabolic level, peptide treatment restored important functions of the gut microbiota that were impaired by WD, as determined by functional pathway analysis of

metatranscriptomics data (Extended Data Fig. 10) and targeted metabolomics. Metabolism of short-chain fatty acids (SCFAs) and amino acids (Fig. 3b and Fig. 3c) were notable.

SCFAs are generated by bacterial fermentation of carbohydrates in the gut and are involved in several microbiota-mediated effects on host metabolism and physiology[12–14]. In the context of atherosclerosis, it is notable that SCFAs can play roles in innate immunity and inflammatory processes through histone deacetylase (HDAC) and/or G-protein coupled receptor (GPCR)-dependent mechanisms[37]. Functional metagenomics analyses suggested that peptide treatment induced changes in enzyme expression levels that would lead to increased butyrate biosynthesis (Fig. 3d). Treatment with c[wLwReQeR] led to higher acetoacetate-CoA transferase levels compared to vehicle (Fig. 3d), which would promote production of butyrate. The observed changes in expression levels for acetoacetate CoA-transferase were ~2.5-fold higher than would be expected based on a random distribution of all changes observed in the RNA-Seq analysis. Indeed, targeted metabolomics analysis of fecal samples taken after a two-week treatment period confirmed that animals treated with peptide c[wLwReQeR] had increased levels of fatty acids containing 4–6 carbons, including butyrate (Fig. 3e). In addition, functional pathway analysis predicted reduced catabolism of tryptophan and phenylalanine (~60% reduction for Trp catabolism, ~20% reduction for Phe catabolism) in CHD or WD peptide-treated animals compared to WD vehicle animals (Fig. 3c). Indeed, targeted metabolomics revealed higher levels of tryptophan and phenylalanine in the feces of peptide-treated animals after a two-week course (Fig. 3f).

Anti-atherogenic effects of peptide treatment

Plasma cholesterol levels and atherosclerotic lesions were strikingly reduced in the mice on WD following peptide treatment. By the two-week time point, oral administration of peptides c[wLwKhShK] and c[wLwReQeR] had reduced the mouse plasma total cholesterol by 37% and 36%, respectively, compared to the untreated WD group (Fig. 4a). There was no analogous peptide-mediated reduction in cholesterol in the CHD-fed mice (Supplementary Fig. 1). In addition, peptide c[wLwReQeR] also reduced plasma triglyceride levels in WD-fed mice by 56% compared to vehicle (Supplementary Fig. 1). Moreover, analysis of plasma lipoprotein fractions by FPLC indicated that the reduction in total plasma cholesterol levels stems from marked reductions in the levels of VLDL and LDL in the peptide-treated WD-fed mice (Fig. 4b). We also confirmed that peptide treatment did not reduce absorption of dietary cholesterol by carrying out a fecal dual-isotope cholesterol absorption assay (Supplementary Fig. 1). At the completion of the 10-week study, analysis of the whole aorta lesion area indicated striking reductions in atherosclerotic lesions of 37% and 48% by peptides c[wLwKhShK] and c[wLwReQeR], respectively (Fig. 4d and Fig. 4e). Similarly, the aortic sinus lesion volume was significantly reduced by 44% and 37%, respectively (Fig. 4f). Microbiota composition analysis indicated that eight microbiota taxa had a positive correlation ($\rho>0.4$) with plasma cholesterol levels, while five taxa were negatively correlated ($\rho<−0.4$) (Fig. 4c). The peptides generally decreased the abundance of the positively correlated taxa and increased the abundance of negatively correlated taxa (Fig. 4c).

Mechanistic control studies

We used two additional peptides (peptide **30**: c[w^{Me}LwR^{Me}eQeR] and peptide **15**: c[fWwYqHhQ]) as negative controls for *in vivo* studies to further probe the link between peptide treatment, remodeling of gut microbiome, and observed phenotypic changes. The control peptide c[w^{Me}LwR^{Me}eQeR] has an identical amino acid sequence as the active peptide **11** (c[wLwReQeR]) but two of its eight backbone amide groups are *N*-methylated (Extended Data Fig. 4), which prevents peptide self-assembly and antimicrobial activity[38]. As opposed to peptide c[wLwReQeR], peptide c[w^{Me}LwR^{Me}eQeR] is incapable of ring stacking and inter-subunit hydrogen bonding because it lacks two amide hydrogen bonding donor sites and suffers from inter-subunit steric encumbrances created by the *N*-methyl moieties (Extended Data Fig. 4)[38]. Therefore, peptide c[w^{Me}LwR^{Me}eQeR] is an interesting control and mechanism of action probe because of its inability to self-assemble into nanotubes and exert similar antimicrobial activity, despite having identical amino acid sequence as the active peptide c[wLwReQeR]. We carried out a 10-week oral dosing study with peptide c[w^{Me}LwR^{Me}eQeR] in *LDLr*^{−/−} mice fed WD, analogous to the studies described above for peptides c[wLwKhShK] and c[wLwReQeR]. Peptide c[w^{Me}LwR^{Me}eQeR] did not reduce total plasma cholesterol levels compared to vehicle controls at 2-wk (Fig. 4a) or 10-wk (Supplementary Fig. 1) timepoints, nor any reduction in aortic sinus plaque volumes at 10-wk (Fig. 4f). As an additional control peptide, we used c[fWwYqHhQ] (peptide **15**), which scored lowest of all peptides tested in the *in vitro en masse* microbiome remodeling (Fig. 1, Supplementary Table 4). As indicated by its low ranking, c[fWwYqHhQ] remodeled the gut microbiota *in vitro*, but not toward a CHD-like state according to our scoring algorithm. Similar to the control peptide c[w^{Me}LwR^{Me}eQeR], peptide c[fWwYqHhQ] did not reduce plasma total cholesterol levels compared to vehicle controls at the 2-wk timepoint (Fig. 4a), after which the study was discontinued. Together, these studies indicated that peptides lacking antimicrobial activity or causing inappropriate remodeling of the gut microbiota did not bring about positive phenotypic changes.

We also treated animals with a cocktail of broad-spectrum antibiotics to deplete the microbiome[39–41]. A key phenotypic marker for atherosclerosis is plasma cholesterol level, which strongly correlates with arterial plaque development. Therefore, we measured plasma cholesterol levels following 2-wk peptide treatment in gut microbiome-depleted *LDLr*_{−/−} mice (Fig.4a and Supplementary Fig. 2). Under these conditions, peptide **11** completely lost its ability to reduce plasma cholesterol levels compared to control peptide **30** or vehicle control (Fig. 4a). Quantitation of bacterial DNA present in fecal pellets showed depletion of the gut microbiota over the course of the study (Supplementary Fig. 2). These studies provide additional support that the mechanism of action involves direct targeting and remodeling of the gut microbiota by the peptides.

Host gene expression induced by microbiome remodeling.

Analysis of mouse liver and ileum (small intestine) samples by RNA-seq (Fig. 5a and Supplementary Fig. 3) revealed that c[wLwReQeR] treatment restored expression of many genes that were downregulated or upregulated in the WD-fed group compared to CHD-fed animals. Most notably, gene ontology analysis indicated that lipid metabolism was upregulated and inflammation- and immune-related responses were downregulated

following peptide treatment (Fig 5b and Supplementary Fig. 3). Expression of cholesterol 7 alpha-hydroxylase (Cyp7a1), the rate-limiting enzyme in the bile acid (BA) biosynthesis pathway, was significantly increased in peptide-treated WD animals (Fig. 5c), suggesting increased conversion of dietary cholesterol to bile acids as a possible mechanism for the reduced plasma LDL cholesterol levels. Indeed, we found that the total bile acid in the peptide-treated vs. control WD-fed mice was two-fold higher in the feces and three-fold lower in the plasma (Fig. 5d). This is consistent with *CYP7A1* transgenic mice having a ~2–3 fold increase in total bile acid pool due to increased hepatic cholesterol catabolism, with associated resistance to diet-induced hypercholesterolemia and atherosclerosis[42].

Cyp7a1 expression is tightly regulated through a feedback control system, in which high levels of dietary cholesterol induce Cyp7a1 expression, while high plasma levels of bile acids act as signaling molecules to inhibit Cyp7a1 expression and bile acid metabolism by activating the farnesoid X receptor (FXR) and the FGF15/19 endocrine axis[17,43]. The gut microbiota can modulate FXR signaling in the gut via bile acid metabolism and processing[17–19]. *FXR*-deficient mice on an *LDLr*–/– background were found to have an improved lipid profile when fed a high-fat diet and were protected against diet-induced obesity and atherosclerosis[44]. Consistent with higher expression of Cyp7a1, we observed that the intestinal expression of FXR and its targets, including fibroblast growth factor 15 (FGF15), were downregulated in peptide-treated animals (Fig. 5c). Furthermore, not only did peptide-mediated remodeling of the gut microbiota alter the total bile acid pool size, it also significantly impacted the relative composition and abundance of certain bile acids in fecal and plasma samples (Supplementary Table 6). For example, the levels of taurine-conjugated muricholic acids (T-α,β-MCAs), known FXR antagonists[23,45] were increased by peptide treatment, as revealed by targeted metabolomics (Fig. 5e). Likewise, the expression of intestinal bile acid transporters Asbt, Mrp2, and Mrp3 were significantly altered by the peptide treatment (Fig. 5c). Together, these data suggest that downregulation of the FGF15 endocrine axis (resulting from the altered processing of bile acids by the remodeled gut microbiota), along with decreased absorption of primary bile acids in the ileum, is likely responsible for maintaining an upregulated bile acid metabolism in the liver, resulting in increased conversion of cholesterol to bile acids that contributes to lower plasma cholesterol levels. It should be noted that T-α,β-MCAs are not found in significant levels in humans, so the observed effects may not be directly applicable to human biology.

Anti-inflammatory and immunomodulatory effects.

Inflammation plays a critical role in the development of atherosclerosis[46,47]. We found that peptide-induced remodeling of the gut microbiome reduced the inflammation caused by WD via several gut microbiota-dependent mechanisms (Supplementary Fig. 3). Some commensal gut bacteria play key roles in the maintenance of gut integrity[48]. Impaired gut integrity can lead to increased leakage of microbiota-derived lipopolysaccharide (LPS) from the gut, causing systemic inflammation that intensifies atherosclerosis pathogenesis[49]. We found that several genes related to tight junctions in the ileum were upregulated by peptide treatment (Fig. 6a and Supplementary Fig. 3), and LPS-lipopolysaccharide response pathways were downregulated (Fig. 5b), suggesting that the defects in gut integrity caused by a WD regimen had been largely mitigated. Indeed, the villi width in the ileum (although not the

length) was significantly increased in peptide-treated animals compared to vehicle controls (Fig. 6b, Fig. 6c, and Supplementary Fig. 3).

We found that peptide-induced gut microbiome remodeling also impacted the immune cell composition in the gut. Helios[+] thymic derived regulatory T cells (tTregs) regulate key pathways for preventing uncontrolled inflammatory responses[50] and play important role in inhibiting the development of atherosclerosis in multiple mouse models[51]. Helios+ tTregs expressing GATA3 play a critical role in tissue repair and intestinal barrier function[52]. Furthermore, the differentiation and maintenance of different subsets of Tregs in the intestine are driven by signals from the gut microbiota, gastrointestinal self-antigens, and dietary antigens[12,53,54]. We found that the composition of Foxp3^{+} regulatory T cell (Treg) population was significantly altered by c[wLwReQeR] treatment (Fig. 6d and Supplementary Fig. 4). We isolated cells from the lamina propria tissue and measured the relative populations of Helios[+] Foxp3+ Tregs to two other subsets of T cells: RAR-related orphan receptor γt (RORγt[+] Foxp3^{+}) Tregs and to proinflammatory RORγt[+] T helper 17 (Th17) cells. Overall, c[wLwReQeR] treatment reduced the absolute number of RORγt^{+} Th17 cells and RORγt[+] Foxp3^{+} Tregs, but maintained the population of regenerative Helios[+] GATA3+ Tregs in *LDLr*^{-/-} mice fed a WD, as indicated by increased Helios[+]/Th17 ratio and increased Helios[+]/ RORγt[+] Treg ratio (Fig. 6d and Supplementary Fig. 4). It is interesting to speculate that since a number of oxysterols serve as natural endogenous RORγt agonists[55], the observed reduction in proinflammatory RORγt^{+} Th17 cells could be related to the altered profile of oxysterols and bile acids resulting from the peptide-induced remodeling of the gut microbiota. Additionally, remodeling of gut microbiome and the increased levels of SCFAs we observed could also be playing a role in the altered immune cell populations via HDAC or GPCR-dependent mechanisms[37].

Interleukin-1β (IL-1β) is a proinflammatory cytokine central to the inflammatory response driven by the interlukin-6 (IL-6) signaling pathway. Inhibition of IL-1β has been shown to reduce the development of atherosclerotic plaques in mice and significantly lower the incidence of recurrent cardiovascular events in humans[46]. In addition to IL-1β, a pathogenic role of IL-1α in vascular inflammation and atherosclerosis has been described[56]. Analysis of liver tissue from WD animals (peptide c[wLwReQeR] treated vs vehicle) using a Luminex assay showed significant reductions in several cytokine and chemokine levels, including IL-1β, IL-1α, IL-6, and TNF-α (Fig. 6e and Supplementary Table 7), providing further support for the systemic anti-inflammatory effects of peptide-induced remodeling of a WD-fed gut microbiome.

Discussion

We developed an *en masse in vitro* screening protocol to select self-assembling cyclic D,L-α-peptides that function as bacterial growth modulators and showed that the oral administration of selected peptides was effective in remodeling, in a targeted manner, a WD-induced gut microbiome *in vivo* to prevent development of atherosclerosis in *LDLr*^{-/-} mice. Our data suggest that the observed reductions in plasma cholesterol levels observed resulted from altered processing of bile acids by the remodeled gut microbiota which in turn led to downregulation of the FGF15 endocrine axis, increasing the expression of cholesterol 7

alpha-hydroxylase (Cyp7a1), and ultimately increasing conversion of cholesterol to bile acids. In addition, cyclic D,L-α-peptide remodeling of WD gut microbiome improved gut barrier integrity, suppressed the production of a number of pro-inflammatory cytokines and chemokines (including IL-1β, IL-1α, IL-6, and TNF-α), increased relative populations of intestinal Helios[+] Treg immune cells, and rebalanced levels of disease-relevant metabolites, such as short-chain fatty acids.

Unraveling the mechanistic underpinning of the observed phenotypic consequences of a given microbiome state is often complex, even when a particular microbiome composition is demonstrably disease-promoting. A given microbiome state might arise as a consequence of the aggregate contributions of a number of microbial species and their associated pattern of active or silenced biological pathways, or from the contributions of only one or a few causative species. We have identified thirteen microbiota taxa in our *in vivo* studies that were positively (eight taxa) or negatively (five taxa) correlated with mouse plasma total cholesterol levels (Fig. 4c). Further studies are needed to definitively parse these issues, such as employing focused peptide library screenings, phage-based bacteria targeting, or gene editing methods. Moreover, transplantation studies with specific microbial consortia in germ-free or antibiotic-depleted animals would be useful in resolving the potential role of specific bacteria to phenotype-associations.

The results of our microbiome and host transcriptome analyses and targeted metabolomics (for short-chain fatty acids and bile acids) point to a number of paths forward for interrogating various mechanistic questions. For instance, the cyclic peptide-induced remodeling of the bacterial community caused extensive reprogramming of the microbiome transcriptome. It will be interesting to study whether the observed transcriptome changes were caused directly by changes in abundance of bacterial species vs. being due to changes in gene expression levels (possibly because of as yet poorly understood changes in interspecies microbial signaling), or some combination of both mechanisms.

In this study we have determined the feasibility of directed remodeling of a gut microbiome for preventing the onset and progression of atherosclerosis in $LDLr^{-/-}$ mice. Further studies in other animal models of atherosclerosis and other microbiome-associated diseases would be necessary to establish the generality, scope, and limitations of the approach.

ONLINE METHODS

Animals and diets.

All procedures involving live animals were approved by the Scripps Research Institute Institutional Animal Care and Use Committee. LDL receptor-null ($LDLr^{-/-}$) mice on a C57BL/6J background bred in house. Unless otherwise noted, all experiments were performed with female $LDLr^{-/-}$ mice. Mice were housed in cages with paper bedding, 4 animals per cage, with a 12 hour light/dark cycle. For studies involving analysis of the gut microbiome, the mice were rotated between cages and co-housed with the mice from different cages for at least one week before the beginning of each study to reduce the variation in the composition of gut microbiome caused by the housing environment. The mice were weaned at 4 weeks of age and were fed *ad libitum* a standard chow diet (Harlan

Teklad 7019) until they were 8–12-weeks old, when they were switched to a high-fat diet (WD) containing 15.8% (wt/wt) fat, 1.25% (wt/wt) cholesterol, and no cholate (Harlan Teklad 94059). At the time that the WD was started, the cyclic peptide was added to the drinking water at a dose of 180 μM and the mice were continued on WD for 10 weeks. The lyophilized peptide was dissolved with sonication in PBS (pH 7.4) containing 1% sucrose, resulting in a clear solution. The drinking water solution was replaced with fresh solution daily for c[wLwReQeR] and c[w^{Me}LwR^{Me}eQeR] or every other day for c[wLwKhShK] and c[fWwYqHhQ]. A control group of mice was fed WD and provided vehicle (PBS with 1% sucrose) drinking water. The mice each consumed approximately 4.0 mL of water per day, and there was no significant difference in water or food consumption between groups. The 10-wk efficacy studies were carried out twice for both c[wLwReQeR] and c[wLwKhShK]. The first studies used standard, non-sterilized diet and handling conditions. To lessen the possibility that bacteria from the environment would affect the gut microbiota composition during the study, in the second set of 10-wk efficacy studies we sought to prevent the introduction of exogenous bacteria to the mice. These studies involved sterilized diet (irradiated LabDiet 5053, UV-irradiated by the manufacturer), sterilized cages/bedding/ water bottles (autoclaved as a unit prior to cage changes), and cages were only opened inside a HEPA filtered animal transfer station for cage changing or to take mouse samples. No differences were observed in the effects of the peptides on plasma total cholesterol levels or atherosclerotic lesions between the standard handling and "sterile" studies. For various follow up mechanistic studies, additional, shorter two- or four-wk studies were carried out for c[wLwReQeR] (including one study conducted by different personnel at a different facility with mice from a different colony, at Bristol-Myers-Squibb in Hopewell, NJ); in each of these studies we observed the same degree of reductions in plasma total cholesterol. Power analysis: For the 2-week plasma cholesterol levels and 10-week plasma cholesterol and atherosclerotic lesion levels, differences of 30% between groups is typical, and the standard deviation within groups is typically less than 25% from the mean. Based on these values, a Power analysis indicates that our group size of n=8 animals/group is sufficient to detect statistically significant changes (alpha = 0.05) with >90% probability.

Cyclic peptide synthesis and preparation.

Peptides were synthesized by using standard Fmoc chemistry with on-resin peptide cyclization. For additional experimental details, please see Supplementary Note. Characterization data for the peptides used in this study are given in Supplementary Table 3.

In vitro cecum culture and peptide screening.

To prepare peptide stock solutions for the assay, a 20 mM peptide stock in DMSO was diluted to 1 mM in 10% sucrose. From that, a 0.64 mM and 0.16 mM peptide dilution in 10% sucrose was prepared. The use of 10% sucrose in the peptide stock was found to prevent the peptides from precipitating over time. The concentration of peptides in stock solutions was calculated based on A280 measurement.

Female *LDLr$^{-/-}$* mice (8–10 weeks of age) were fed a WD for two weeks. Cecum harvest and all assay steps were performed under anaerobic conditions (Coy Laboratory anaerobic chamber). Cecum contents from three co-housed mice were pooled for the assay to provide

enough material and to minimize the individual variation in gut microbiome. Cecum contents were suspended in PBS (1.5 ml PBS per 100 mg of cecum content). The mixture was vortexed for 5 min and left to settle for 5 min. A 1.0 ml aliquot of the supernatant from the settled cecum suspension was removed and centrifuged (2,700 g for 5 min), and the bacterial pellet was flash frozen for use as the non-cultured control. A 10 ml portion of the supernatant from the settled cecum suspension was diluted with 115 mL Chopped Meat Carbohydrate Broth (BD 297307) (1:12.5 dilution) to give a total of 125 ml of inoculated media that was used for *in vitro* peptide screening. We found that Chopped Meat Carbohydrate broth maintained higher bacterial diversity during a 48 h *in vitro* culture compared to other media that were examined. The assay was initiated immediately after preparing the inoculated media by mixing 150 μl of a peptide stock (at either 0.64 mM or 0.16 mM) with 1.35 ml of inoculated media in 5 ml snap-cap culture tubes to give 1.5 mL of each assay sample at a final peptide concentration of 64 μM or 16 μM. To monitor the overall bacterial growth profile during the assay, 0.2 ml of each assay sample was removed to a 96 well microplate in a plate reader incubated at 37 °C and OD_{600} was measured at 1-hour intervals. The remaining 1.3 mL of each assay sample was incubated at 37°C for 20 h, after which time the bacterial DNA was harvested and isolated with Microbial DNA isolation kit (Mo Bio) following the manufacturer's instructions. In general, the overall bacterial growth profiles, as monitored by increase in OD_{600}, were similar for the peptide-treated samples compared to that of the untreated control sample. In all peptide treatments, the final OD_{600} was at least 80% of that observed for the untreated control. Insofar as OD_{600} is a proxy for bacterial density, these data support that the overall bacterial density in the peptide-treated conditions remained similar to that of the untreated control.

Following the *in vitro en masse* assay, peptides were scored/ranked as follows. First, we removed peptide sequences that exhibited broad-spectrum antibacterial activity, as defined by causing a 95% reduction of observed reads compared to the vehicle-treated control for 20 species. Of the 29 peptides screened, 6 were eliminated due to broad antibacterial activity. The remaining 23 compounds were then ranked based on the degree to which they suppressed the growth of the 19 bacterial species that increased in abundance in WD-fed mice compared to CHD-fed mice (found in Supplementary Table 1). These 19 targeted bacterial species were identified as follows: out of the 54 bacterial genera that showed significant (adjusted p<0.05) changes in abundance in *LDLr*⁻/⁻ mice fed CHD vs. WD (Supplementary Table 1), 40 genera decreased while 14 genera increased in abundance with WD feeding. Within the 14 genera that increased in abundance, there were 19 bacterial species that were also present in our *in vitro* culture system. Peptides were scored by summing the observed changes in abundance for each of the identified bacteria, with shifts toward the CHD state being considered positive and shifts away being negative. Compounds scored highly when they reduced the levels of the 19 bacterial species (lowest summed differences in relative abundance). The peptide ranking is found in Supplementary Table 4.

MIC assays against individual bacterial strains.

For details of *in vitro* MIC assays against nine representative laboratory strains of gut bacteria, see Supplementary Note.

Feces sample collection and DNA extraction.

The feces samples were freshly collected after 2, 6, and 10 weeks of treatment, snap-frozen, and stored at −80°C. Microbial genomic DNA was isolated with PowerSoil DNA isolation kit by following manufacturer's instructions (Mo Bio).

16S rRNA gene sequencing and processing.

PCR amplicons of the V3-V4 16S rRNA region were amplified and sequenced using an Illumina MiSeq platform. For each sample, duplicate 25 μl PCR reactions were performed, each containing 50 ng of purified DNA, 12.5 μl 2X KAPA HiFi HotStart ReadyMix (Kapa biosystem), and 0.15 μM of each primer designed to amplify the V3-V4 region: forward primer (5'-AATGATACGGCGACCACCGAGATCTACACTCTTTCCCTACACGACG CTCTTCCGATCTNNNNNNNNNNNNNNACTCCTACGGGAGGCAGCAG-3') and reverse primer (5'-CAAGCAGAAGACGGCATACGAGATNNNNNNNNNNNNNGTGACTGGA GTTCAGACGTGTGCTCTTCCGATCTnnnnnnnnnnnGGACTACHVGGGTWTCTAAT-3'). A unique 12-base sequence (N's) was included for sample identification. We also included unique molecular identifiers (n's) to correct PCR duplication artifacts during the library preparation. Cycling conditions were 98°C for 2 min, followed by 20 cycles of 98°C for 10 s, 60°C for 30 s, and 72°C for 45 s. A condition of 72°C for 5 min was used for the final elongation step. Replicate PCR samples were pooled, and amplicons were qualified with Quant-iT dsDNA Assay kit (ThermoFisher). Each sample was combined at an equimolar amount before DNA purification with Agencourt AMPure XP (Beckman Coulter). The completed library was sequenced on an Illumina MiSeq platform following the Illumina recommended procedures, to an average depth of $177,286 \pm 33,033$ read pairs per sample.

16S rRNA gene sequencing data analysis.

We used custom python scripts to demultiplex sequencing reads based on the second barcode index and remove PCR duplication artifacts found using unique molecular identifiers prior to analyzing sequences using the mothur[57] (version 1.36.1). We developed a custom analysis pipeline based on the MiSeq SOP published by the curators of mothur. Briefly, contigs were generated by combining forward and reverse paired-end reads using the mothur make.contigs command. $177,286 \pm 33,033$ contigs were generated per pair (11,346,311 total). The contigs were filtered based on their length (440–480bp for V3-V4 region), and any contigs with ambiguous bases were removed. Redundant contigs were then consolidated from the remaining 9,653,596 contigs, and 1,176,445 unique contigs were then aligned to a reference database (SILVA non-redundant dataset v119). The contigs that didn't align properly based on position of alignment and those with homopolymers of length > 8 were removed before the downstream analysis. We performed a pre-clustering step to cluster reads up to 2 bp apart and removed all chimeric sequences. Finally, we used a k-mer based method to classify the sequences to individual taxonomic groups to get counts per group. Scripts used for calculating the Chao1 index can be found at: https://github.com/bmolparia/ species_richness. Furthermore, we performed statistical analysis on the 16S data using DESeq2[58] to identify significantly altered bacterial genera (adjusted p-value < 0.1) and compare the distribution of various groups using principal-component analysis. Shannon diversity was calculated using the following equation, where H is the Shannon diversity

index, G is the number of genera present in each sample, and p_i is the relative abundance of each genera within the sample:

$$H = -\sum_{i=1}^{G} p_i \ln(p_i)$$

Measurement of plasma cholesterol and liver enzyme activities.

Plasma cholesterol and liver enzyme activities were determined using enzymatic assays. See Supplementary Note for additional details.

Pharmacokinetics and quantitation of c[wLwReQeR] levels in plasma and feces.

The cyclic peptide was extracted from plasma or feces and measured by using reverse-phase HPLC coupled with mass spectrometry selected ion monitoring. See Supplementary Note for additional details.

In vivo cholesterol absorption assay.

To assess the effects of c[wLwReQeR] on intestinal absorption of cholesterol, a dual fecal isotope ratio method was used. See Supplementary Note for additional details.

Plasma lipoprotein profile.

Pooled plasma (240 μL total, 30 μL from each, n = 8 fasted mice per group) from the two-week blood draw was used for fast protein liquid chromatography (FPLC) analysis. Lipoproteins were separated by using 3 Superdex 200 10/30 columns connected in series (GE Healthcare). The plasma was centrifuged at 11,000 rpm for 10 min at room temperature to remove particulates (floating material was gently mixed into liquid before removing the supernatant for FPLC injection). 200 μL of the pooled plasma was injected on the system eluted with 10 mM tris-HCl buffer, pH 7.4, containing 1 mM EDTA and 150 mM NaCl; a flow rate of 0.5 ml/min and fraction size of 0.5 mL were used.

Analysis of atherosclerosis.

Atherosclerotic lesion severity was assessed by *en face* analysis of the entire mouse aorta and analysis of lesions in the aortic root (heart sinus). See Supplementary Note for additional details.

Antibiotic-induced gut microbiota depletion study.

We used a gut microbiota depletion procedure described by Staley et al[59]. Female LDLr−/− mice (n = 35), 8–20 weeks of age were randomized twice between 7 cages in groups of 5 mice/cage to equalize the microbiota and even out age spread. Housing units (cage, bedding, and water bottles) were autoclaved over the entire course of the study. Food was irradiated by vendors. Mice were fed standard chow diet (PicoLab Rodent Diet 20, #5053, % Kcal from: protein 24.65%, carbohydrate 62.14 %, fat 13.20 %) prior to the study and then switched to a high fat diet (Envigo #TD.94059, % Kcal from: protein 20.4 %, carbohydrate 42.7 %, fat 36.9 %) on day −21. The antibiotic cocktail was prepared fresh daily one day

prior to consumption, stored at 4°C, and replaced daily. The cocktail consisted of three nonabsorbable antibiotics each at 1 mg ml^{-1} in the drinking water (ertapenem sodium salt, neomycin sulfate, vancomycin hydrochloride). Peptides were dissolved in sterile 1.2% sucrose prior to the study and stored at −20°C and then diluted with 10X PBS to final 1X. PBS was used as vehicle control. Final concentrations of peptide were 180 μM in drinking water (corresponding to a dose of ~30 mg kg^{-1} day^{-1}). The timeline of the study is shown in Supplementary Figure 2. Blood and fecal samples were collected at each timepoint and mice were weighed. One cage received no treatment as a control. DNA was isolated from the fecal samples using a DNeasy Powersoil kit (Qiagen). Genomic DNA was measured using a nanodrop 2000. 5 ng of gDNA was amplified using forward and reverse 16Sv3–4 primers (as described elsewhere). Amplicon concentrations were measured using a Qubit dsDNA HS (High Sensitivity) Assay Kit (Thermo Fisher). Equal amounts of each amplicon were combined into one of two libraries (each library containing either 2 or 3 of the 5 replicates from each treatment group, n = 112 or 114 samples, respectively) and cleaned up using Ampure XP beads (Beckman Coulter). Purity was checked using Bioanalyzer High Sensitivity DNA kit (Agilent) and the libraries were sequenced using an Illumina MiSeq (2×300 kit) using a full flow cell run with 20% added PhiX.

Bacterial RNA-seq sample preparation and sequencing.

RNA-seq was carried out using a single sample from each group to generate profiling information that could be validated and confirmed by using qPCR and metabolomics analyses. Total bacterial RNA from feces samples was isolated with ZR Soil/Fecal RNA MicroPrep (Zymo research) following the manufacturer's instructions. Briefly, the sample was suspended in RNA lysis buffer and lysed by the mixer (Retsch). The supernatant was transferred to a RNA-binding column and washed several times with RNA wash buffer. In-column DNaseI digestion at 25°C for 15 min was performed to eliminate DNA contamination in the sample. The presence of genomic DNA contamination was assessed by PCR with universal 16S rRNA gene primers. Before RNA-seq library preparation, rRNA was removed from 2 μg of total bacterial RNA with Ribo-Zero Bacteria kit (Illumina). 100 ng of purified RNA was used for RNA-seq library preparation as described previously[60]. The cDNA was synthesized by reverse transcription with SuperScript III (Life technologies) and second-strand synthesis (New England Biolabs). The sequencing library was generated from purified cDNA with Nextera XT DNA library preparation kit (Illumina) and amplified by PCR. Cycling conditions were 72°C for 3 min, 95°C for 30 s, followed by 16 cycles of 95°C for 10 s, 55°C for 30 s, and 72°C for 30 s. A condition of 72°C for 5 min was used for the final elongation step. Libraries with different indexes were pooled and sequenced on an Illumina NextSeq at the Scripps Research Institute next generation sequencing core. 4,453,883, 8,956,883, and 9,166,765 reads were generated from the CHD, WD, and WD + c[wLwReQeR] samples, respectively. Of these reads, 1,367,533 were mappable for CHD (30.7% of total generated reads), 4,411,184, were mappable for WD (49.2% of total generated reads), and 4,470,591 were mappable WD + c[wLwReQeR] (48.8% of total generated reads).

Functional analysis of bacterial RNA-seq data.

We used BWA (version 0.7.12) read alignment program[61] and a custom-built bacterial reference database, which contains 4,700 bacterial genomes from NCBI NR sequence database, to map RNA-seq reads. The reads aligned to individual bacterial genes were counted using HTSeq count[62] (version 0.6.0) and the counts were further normalized based on size factors estimated using the median of the ratios of observed counts method as described previously[63]. The proteins predicted by RNA-seq read alignment were annotated with DIAMOND[64] (version 0.8.26) using the NCBI nonredundant (NCBI-nr) database[65] and the default setting (BLASTX e value $< 10^{-3}$, bit score > 50). For query genes with multiple matches, the annotated reference gene with the lowest e value was chosen. The functional analysis was performed by MEGAN[66] (version 5.11.3) and KEGG analyzer was used to determine read counts in different metabolic pathways from each group. The aggregate expression level changes for sequences within a given function were normalized before the comparison between each group.

SCFA and amino acid measurements.

Fecal SCFA and amino acid content were measured by targeted metabolomics. See Supplementary Note for additional details.

Mouse RNA-seq sample preparation and sequencing.

Mouse tissues were harvested after 2 weeks of treatment, stored in RNAlater, and snap-frozen. 20–30 mg of mouse tissue was used for RNA extraction with RNeasy Mini Kit (Qiagen) following the manufacturer's instructions. Ribosomal RNA was removed from total RNA with Ribo-Zero Gold rRNA removal kit (Illumina). Strand-specific RNA-seq libraries were constructed as described previously[67]. Libraries with different barcodes were pooled and single-end sequencing (75bp) was performed on an Illumina NextSeq at the Scripps Research Institute next generation sequencing core.

Mouse RNA sequencing data analysis.

After ribosomal RNA sequences were removed, the RNA transcripts were quantified using RSEM[68]. Differentially expressed genes were identified by DESeq2[58] and significantly changed genes were selected using a cutoff of adjusted p-value < 0.1, comparing peptide-treated animals (n=3) to vehicle-control animals (n=3) for each group (CHD or WD-fed animals). Enrichment of Gene Ontology terms and categories was performed with DAVID 6.8[69,70].

Quantitative real-time PCR.

To validate selected gene expression results, qPCR reactions were carried out. Mouse livers were harvested two weeks after peptide treatment and total RNA was extracted using RNeasy Mini (Qiagen) following manufacturer's instructions. Reverse transcription was performed for 1 h using random priming (Promega). qPCR reactions (0.5 μl cDNA, 0.2 μM each primer, SYBR green Master Mix (Kapa biosystems)) were performed on a Bio-Rad CFX384 Touch Real-Time PCR detection system, using primers specific for each gene (Supplementary Table 8). Data were normalized to loading controls (16S and β-actin).

Bile acid quantifications.

Total bile acids were measured enzymatically using a total bile acid assay kit (Cell Biolabs) following manufacturer's instruction. Individual bile acids were measured using targeted metabolomics. See Supplementary Note for additional details.

Quantification of regulatory T cells.

Lamina propria (LP) immune cells from the small intestine were isolated using a lamina propria dissociation kit and quantified using flow cytometry. See Supplementary Note for additional details.

Statistical analysis.

Data are expressed as the mean ± S.D. Statistical significance was determined by analysis of variance (ANOVA) or Student's t-test (details are provided in corresponding figure legends), as determined by using GraphPad Prism software (version 8.3.1). p values <0.05 were considered as statistically significant for *in vivo* animal study.

Data availability.

Source Data for quantifications mentioned either in the text or shown in graphs are available by request from the corresponding authors. RNA-seq data have been deposited in the Gene Expression Omibus under accession GSE104915; 16S rRNA sequencing reads have been deposited in MG-RAST under accession 93528, 93529, and 93586.
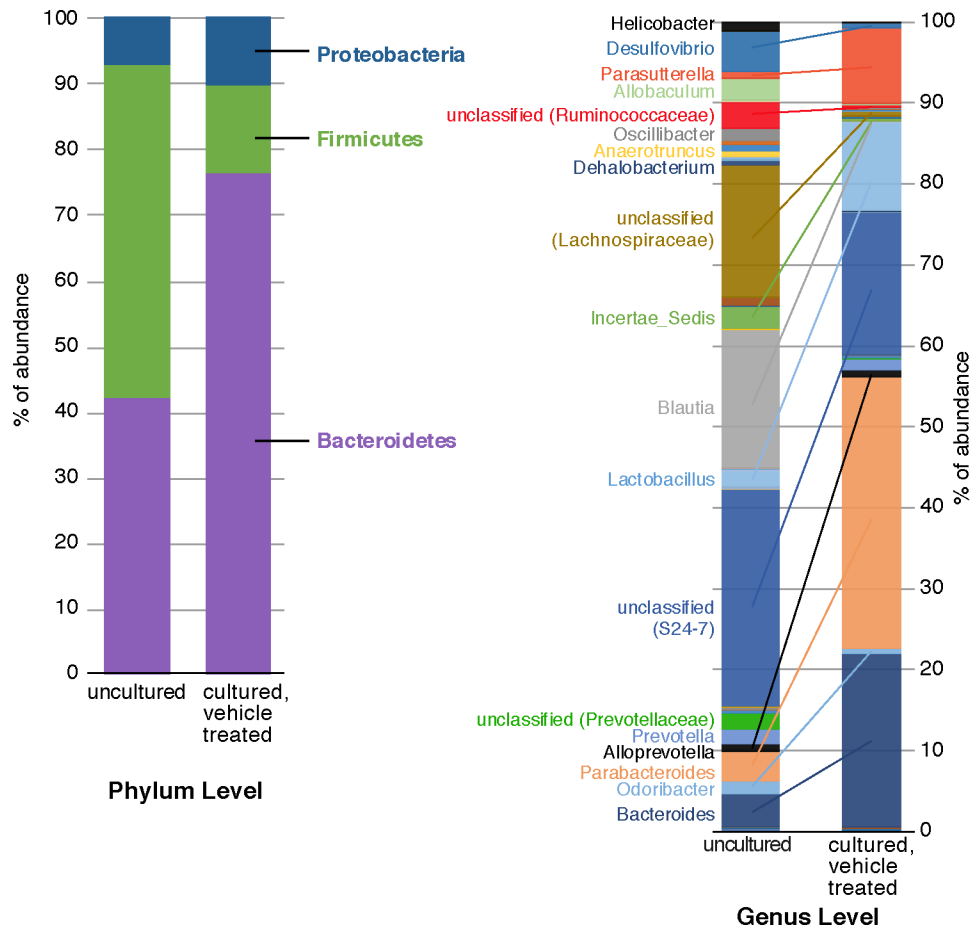
Extended Data
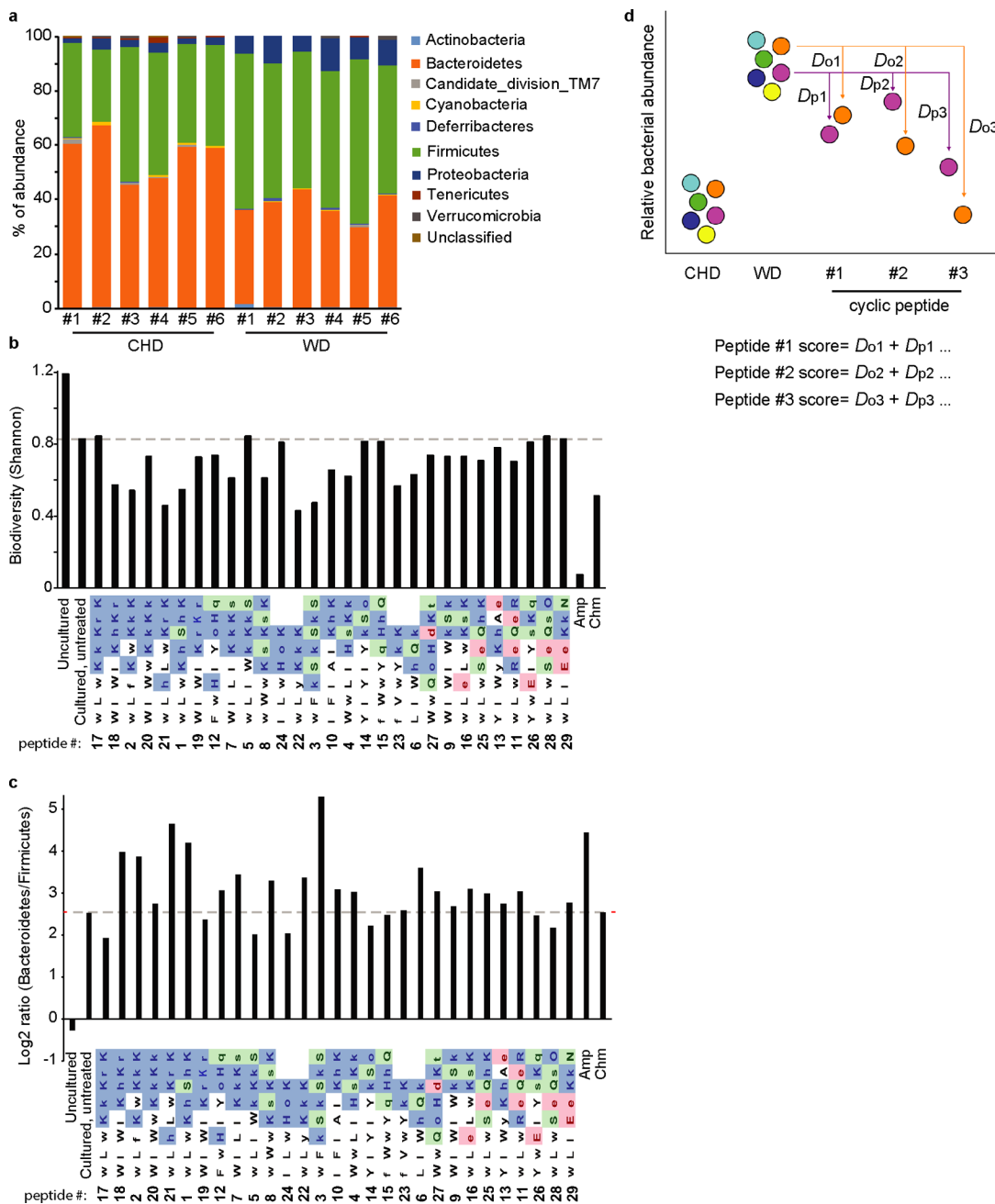
**Extended Data Fig. 1. Changes in gut microbiota composition due to WD feeding in vivo and peptide treatment in vitro.**

a, The composition of gut microbiota from fecal samples of *LDLr*$^{-/-}$ mice after 2-wk feeding of CHD or WD. **b**, The alpha diversity (biodiversity) of gut microbiota from cecum of *LDLr*$^{-/-}$ mice cultured *in vitro* for 20 h with the indicated cyclic peptides (16 μM). Two broad-spectrum antibiotics, 4 μg/mL ampicillin (Amp) and 8 μg/mL chloramphenicol (Chm), were used as positive controls in this assay. The dashed line indicates the biodiversity in the cultured, untreated control sample. **c**, The ratio of bacteroidetes to

firmicutes in the *in vitro* cultured microbiota samples after cyclic peptide treatment. The dashed line indicates the ratio of bacteroidetes to firmicutes in the cultured, untreated control sample. **d**, Schematic diagram of the distance-based algorithm for scoring peptides following the *in vitro en masse* assay. The algorithm considers only the bacteria that increased in abundance under WD feeding compared to CHD feeding (species o, p, etc.). Peptide treatment could cause abundance of those bacteria to further increase (away from the CHD state), to decrease (toward the CHD state), or remain unchanged. Peptides were scored by summing the observed changes in abundance for each of the identified bacteria (Do1, Dp1, etc.), with shifts toward the CHD state being considered positive and shifts away being negative.

Extended Data Fig. 2. Composition of the cultured gut bacteria community from the *en masse in vitro* screen compared to the uncultured community.
The major observed taxa at the phylum and genus levels are labeled.
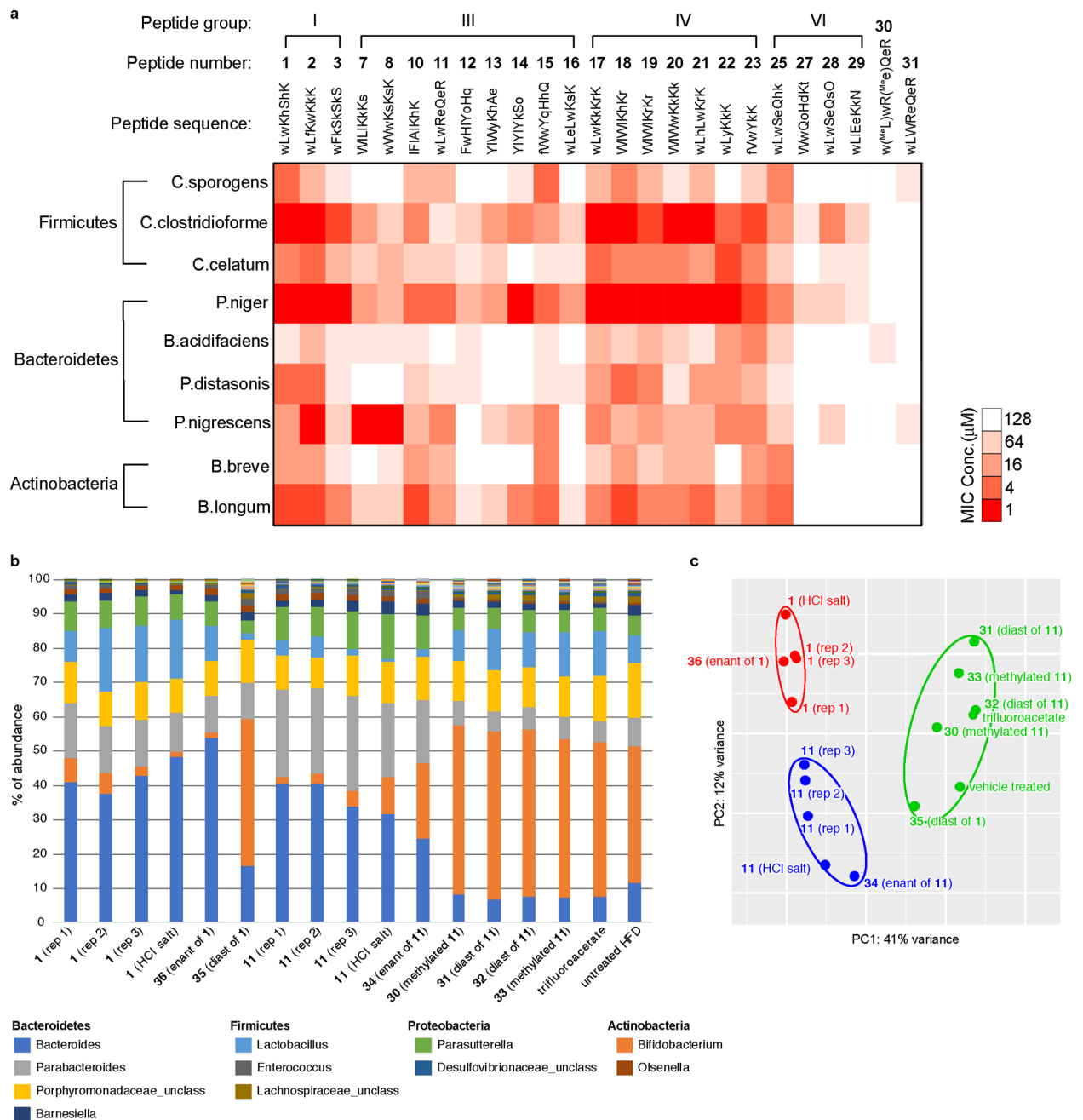
Extended Data Fig. 3. Cyclic D,L-α-peptides can affect the growth of individual bacteria or the composition of bacterial communities *in vitro*.

a, Heatmap showing minimum inhibitory concentration (MIC) values for the screened peptides against selected bacteria *in vitro*. The MIC for a given peptide against a given bacteria was defined as the lowest concentration of peptide that inhibited >90% of growth; lower MIC values correspond to greater antibacterial activity. The peptide groups shown at the top of the heatmap correspond to those identified from a pairwise comparison of the activities of different cyclic peptides in the *en masse* assay, each of which affected the microbiota differently from the other groups. Similar to the result from the *en masse* screen, peptides from different clusters showed the distinct effects against individual gut bacterial

species in the MIC assay. Peptide c[wLwKhShK] (**1**), from peptide group I, broadly affected most of the bacterial species tested to some degree. In contrast, c[wLwReQeR] (**11**), from peptide group III, differentially affected bacterial species from Firmicutes and Bacteroidetes. Peptide **30** is an *N*-methylated analog of peptide **11**, whereas **31** is a diastereomer of peptide **11**. Because these disatereomeric and backbone *N*-methylated analogs cannot self-assemble into nanotubes, these peptides serve as mode-of-action controls that support the expected mechanism of bacterial growth modulation being dependent on peptide self-assembly and bacterial membrane activity. **b**, Bar graphs showing the relative abundance (genus level) of *in vitro en masse* screening samples treated with peptides **1**, **11**, or their analogs as mode-of-action controls. Peptides **1** and **11** were each screened in triplicate in the screen. 'HCl salt' refers to peptides that had been converted from the trifluoroacetate counterion salt (obtained after preparative HPLC) to the hydrochloride salt. 'Trifluoroacetate' refers to a sample treated with sodium trifluoroacetate (1 mM). The peptide HCl salts and trifluoroacetate samples were used to establish that trifluoroacetate itself (present as counterions with the screened peptides) does not affect microbiota composition. **c**, Principal component analysis for *in vitro en masse* screening samples treated with peptides **1**, **11**, or their analogs as mode-of-action controls (n = 3 independent samples each for peptide **1** and peptide **11**, n = 1 for the other treatments shown). As expected, peptides **1** and **11** promoted distinct microbiota remodeling activity that were clustered for the replicate treatments along with their corresponding HCl salt and enantiomeric peptide (which can self-assemble). On the other hand, the diastereomeric or *N*-methylated analogs (which cannot self-assemble) did not substantially affect microbiota growth, as demonstrated by their clustering with the vehicle-treated and trifluoroacetate control samples.
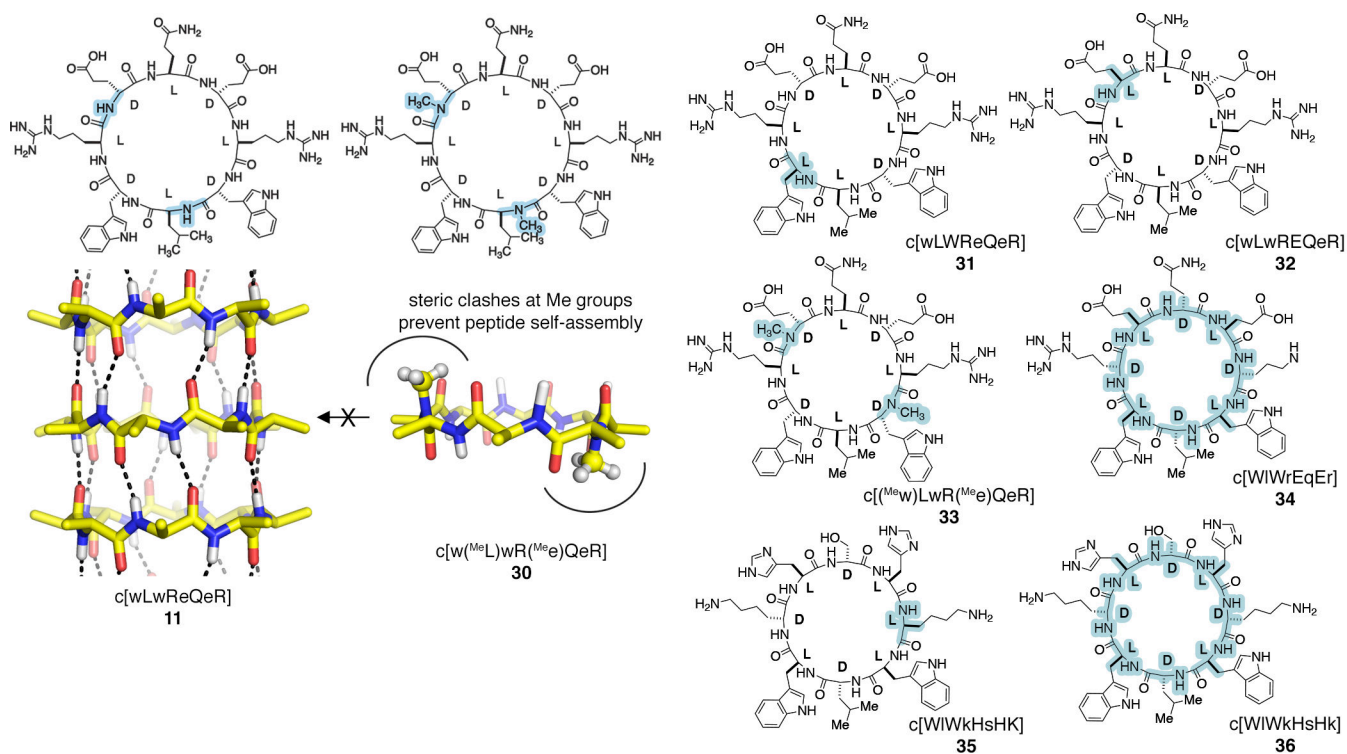
Extended Data Fig. 4. Design rationale and structures for mechanism-of-action control peptides.
In the absence of backbone *N*-methylation, as in peptide **11**, the flat ring-shaped cyclic conformation favors peptide stacking and inter-subunit backbone hydrogen bonding, giving rise to tubular ensembles that can perturb transmembrane ion gradients to exert antimicrobial activities. Backbone *N*-methylation on each face of the macrocycle, as in peptide **30** and **33**, creates a dual effect that prevents peptide self-assembly and membrane/antimicrobial activity. The modified ring structure not only lacks two amide hydrogen bonding sites but is also incapable of ring stacking and inter-subunit hydrogen bonding as a result of steric clashes by the *N*-methyl moieties. Therefore, peptides **30** and **33** are interesting control and mechanism of action probes because of their inability to self-assemble and exert membrane and antimicrobial activity, despite having identical amino acid sequence as peptide **11**. For clarity, side chains are omitted from the molecular models shown. Likewise, switching the stereochemistry of one of the amino acid side chains yields a diastereomer of the parent peptide. Diastereomers, such as peptides **31**, **32**, and **35** lack the flat ring-shaped cyclic conformation that favors peptide stacking, thus diminishing the propensity for self-assembly. On the other hand, the alternating arrangement of D- and L-amino acids is present in enantiomers of the parent peptides, such as **34** and **36**, producing the flat ring-shaped cyclic conformation that favors peptide stacking.
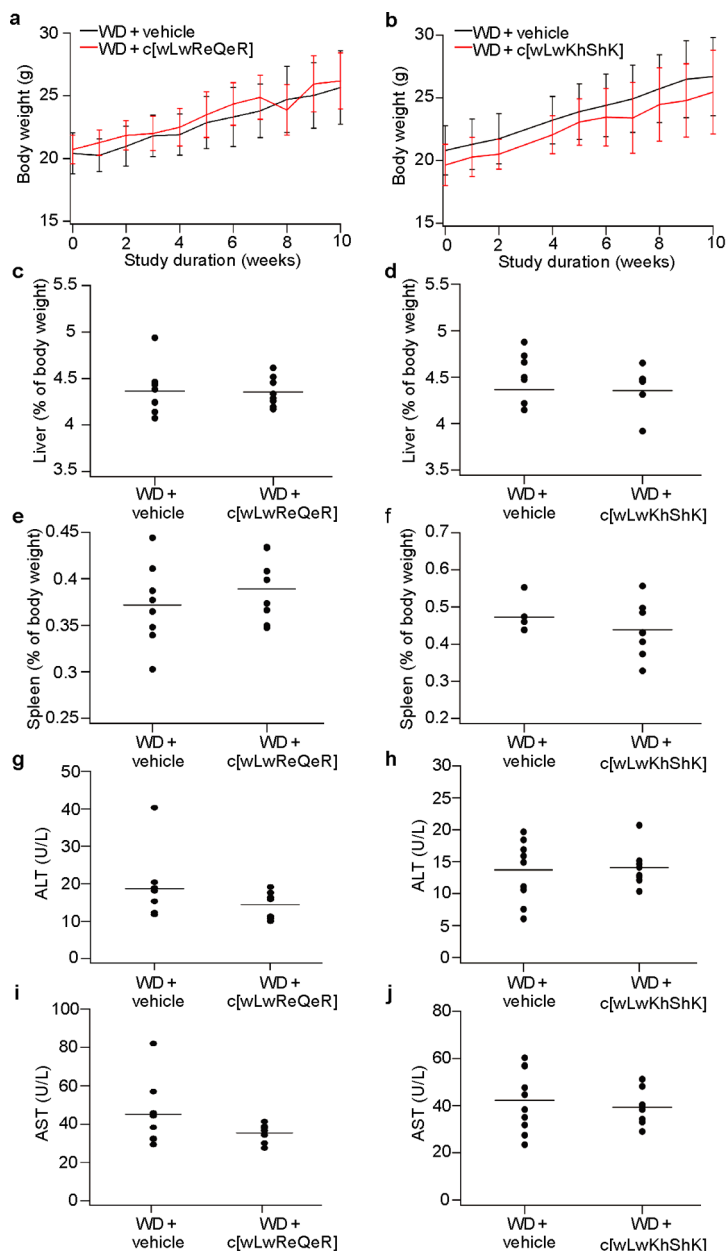
Extended Data Fig. 5. Daily oral administration of cyclic peptides c[wLwReQeR] and c[wLwKhShK] for 10 weeks showed no toxicity *in vivo*.
a,**b**, The body weights of the mice during the 10-week cyclic peptide treatments did not differ from vehicle controls. Data are shown as mean ± SD. **c-f**, The liver weights (**c,d**) and spleen weights (**e,f**) of peptide-treated animals did not significantly differ from vehicle controls. **g-j**, Plasma levels of alanine aminotransferase (ALT) and aspartate aminotransferase (AST) of peptide-treated animals did not significantly differ from vehicle controls, indicating the cyclic peptides did not cause liver damage or injury in the mice. In panels **c-i**, the horizontal line shows the mean. In all panels, n = 8 mice for WD + vehicle group in the c[wLwReQeR] study; n = 7 mice for WD + c[wLwReQeR] group; n = 9 mice

for WD + vehicle group in the c[wLwKhShK] study; n = 7 mice for WD + c[wLwKhShK] group.
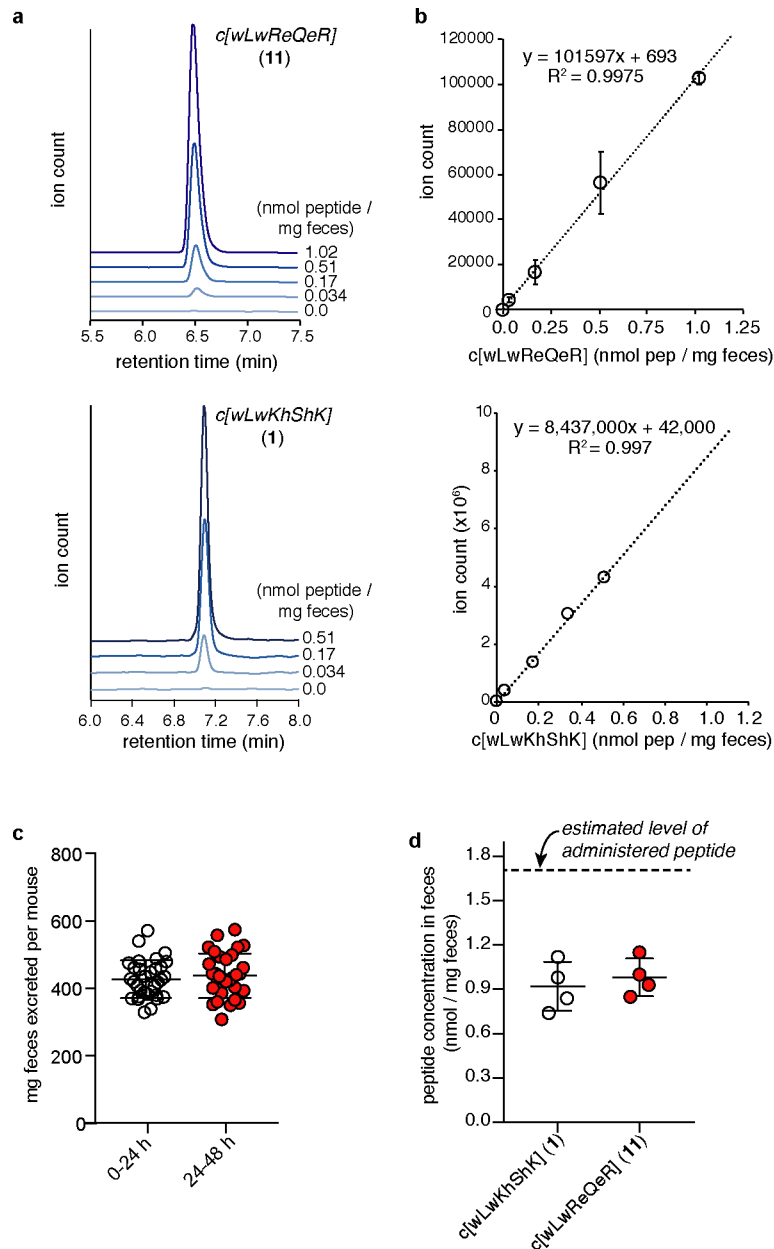

Extended Data Fig. 6. Quantitation of peptide levels in feces of treated mice.
a, Representative LCMS selected ion traces used to generate standard curves for determining the concentration of peptides in extracted mouse feces. The traces correspond to ion 1181.8 ([M-H]$^{1-}$) for c[wLwReQeR] and ion 368.2 ([M + 3 H]$^{3+}$) for c[wLwKhShK] at the peptide concentrations shown. Standard curves were generated from two independent extractions. **b**, Standard curves used for quantitation of c[wLwReQeR] and c[wLwKhShK] concentrations in the feces of treated mice. Data are shown as mean ± SD of n = 2 independent replicates for each concentration. **c**, Measured quantities of feces (dry weight after lyophilization of

fecal pellets) excreted by individually-housed WD-fed $LDLr^{-/-}$ mice over 24-h periods (n = 32). Data are shown as mean ± SD. The observed mean ± SD value was 432 ± 61 mg feces/day/mouse. **d**, Measured levels of fully intact peptides in the 5-wk fecal samples of treated $LDLr^{-/-}$ mice (n = 4 animals per group). Each circle represents the average of duplicate measurements from a single animal. Data are given as mean ± SD of the values for the 4 animals in each group. The observed fecal concentrations of the fully-intact peptides of 1.0 ± 0.1 nmol peptide/mg feces and 0.9 ± 0.2 nmol peptide/mg feces for c[wLwReQeR] and c[wLwKhShK], respectively, represent greater than 50% of the level that would be expected assuming all of the administered peptide was excreted in the feces (~1.7 nmol peptide/mg feces). The estimated maximum fecal peptide concentration that would be expected assuming all of the administered peptide was excreted in the feces was calculated from the known concentration of peptide administered in the drinking water (0.18 mM), the average daily volume of treated drinking water consumed by each mouse (4.5 mL), and the average daily amount of feces excreted by each mouse (432 mg).
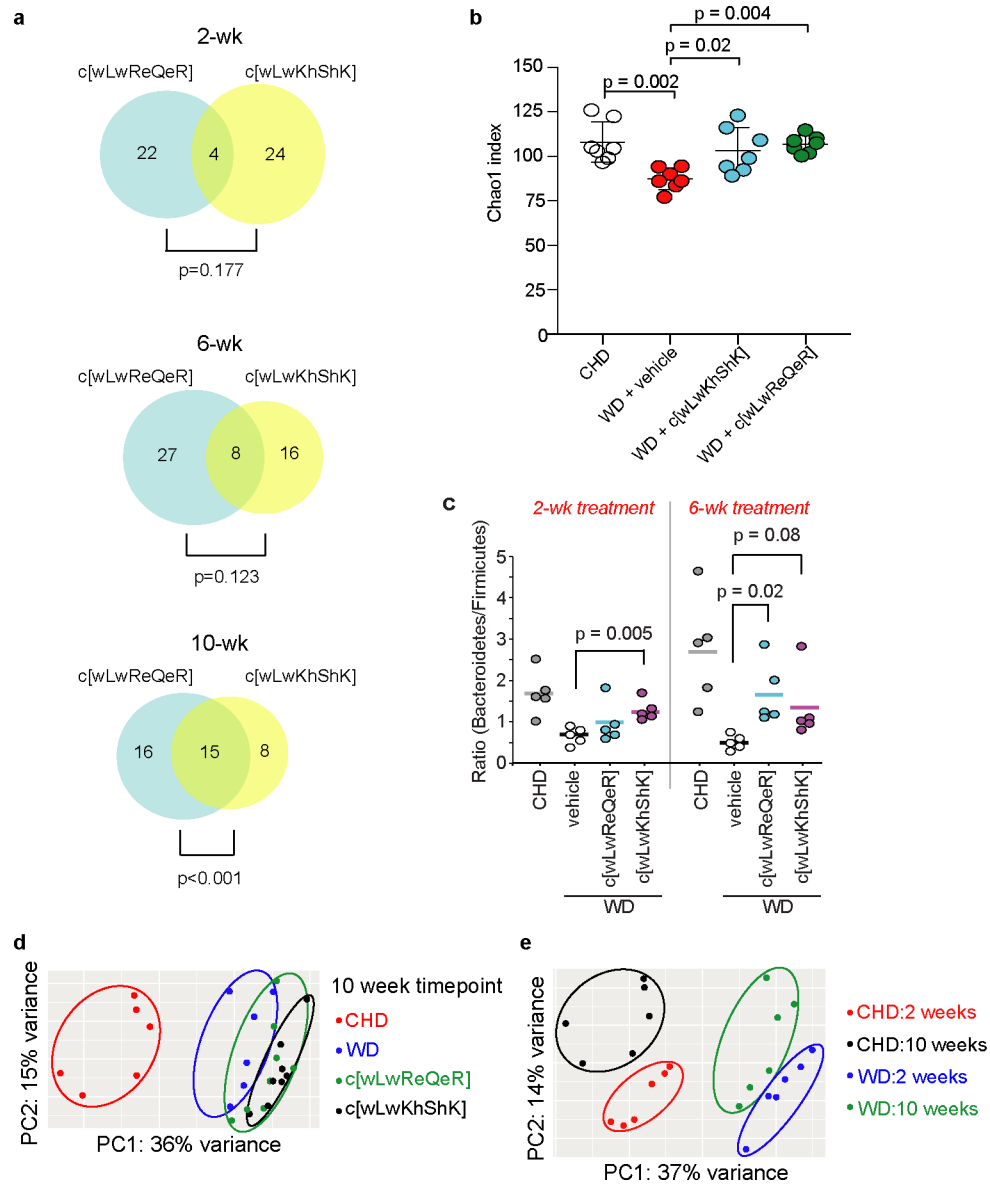
Extended Data Fig. 7. Effects of peptide treatment on bacterial composition and richness over time.

a, Comparative effects of cyclic D,L-α-peptide-mediated remodeling of gut microbiota in $LDLr^{-/-}$ mice over the course of a 10-wk study. The time course analysis shows the number of genera in feces samples that were significantly changed in abundance relative to vehicle treatment at the timepoint indicated (n = 7 animals for all groups). The two peptides initially targeted different bacterial genera (out of 50 total genera that were significantly changed in abundance by treatment with the two peptides [adjusted p-value < 0.1, as determined by a hypergeometric test], only four genera were affected in common by both peptides after 2-wk peptide treatments). Over the course of the study, the remodeled gut microbiome community induced by peptide treatments became more similar (after 10-wk treatment, 15 bacterial genera were inhibited in common out of 39 total genera affected by the peptides). **b**, Effect of peptide treatment on richness (Chao1 index) of gut microbiota from WD-fed $LDLr^{-/-}$

mice (n = 7 animals for all groups). Samples were taken from feces after a 2-wk treatment period. The scatter plot is shown with mean ± SD. *p* values were determined by ANOVA. **c**, Peptide treatment shifted the ratio of Bacteroidetes to Firmicutes in feces of WD-fed mice toward that of the CHD-fed controls over the time periods shown. Scatter plots are shown with mean. *p* values were determined by two-tailed Student's t-test. n = 5 per group. **d**, Principal-component analysis of genera abundance for CHD-fed mice and for WD-fed mice treated with peptides or vehicle (n = 6 animals each for CHD and WD groups; n = 8 animals each for c[wLwReQeR] and c[wLwKhShK] groups, data shown for 10-wk timepoint). **e**, Principal-component analysis of genera abundance for WD/vehicle and CHD/vehicle mice after 2-wk and 10-wk (n = 6 per group).
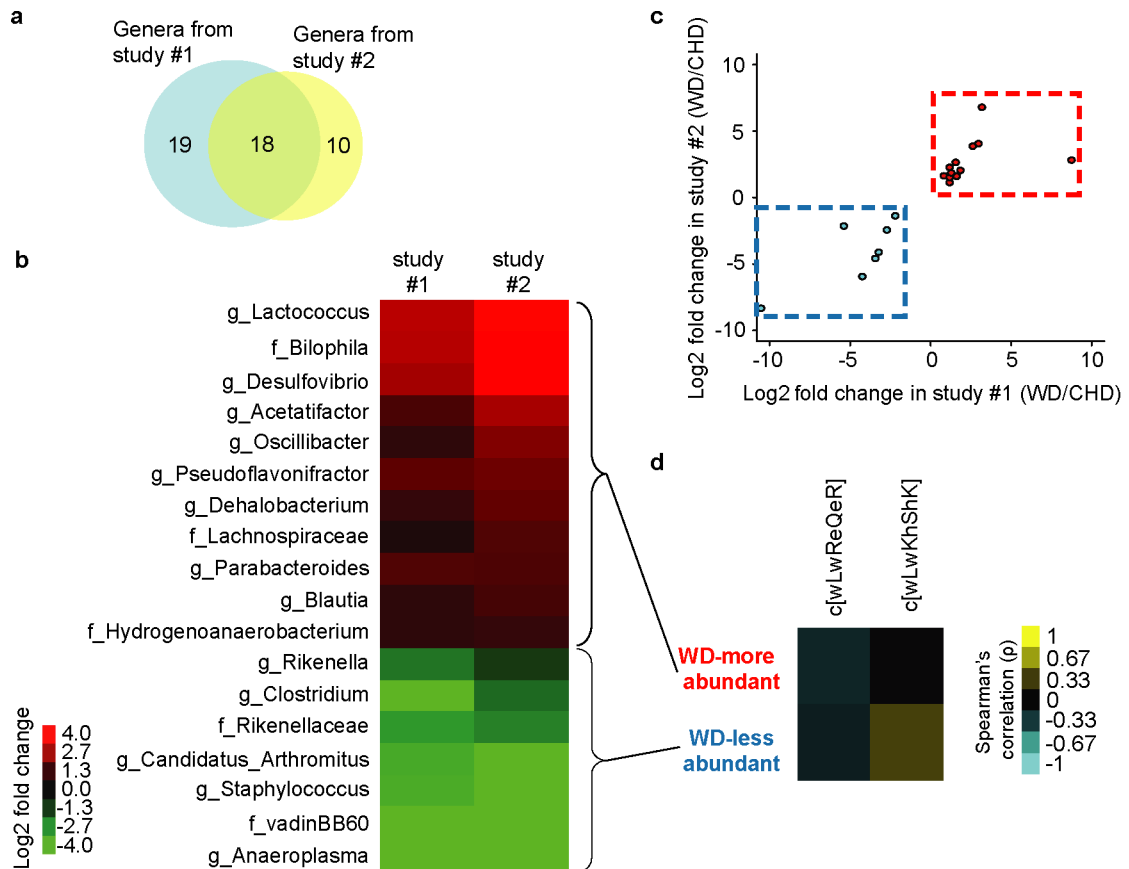
Extended Data Fig. 8. *In vivo* remodeling effects of cyclic D,L-α-peptides on the gut microbiota genera for which WD feeding caused significant changes in abundance compared to ChD.
a, Comparison of the bacterial genera observed to significantly differ (adusted p-value < 0.1, as determined by DESeq2 using a two-sided Wald test with adjustment for multiple comparisons using the Benjamini-Hochberg method) between WD-fed mice compared to CHD-fed mice from two independent animal studies (in both studies, n = 9 animals for CHD group and n = 8 animals for WD group). 18 genera were observed to differ significantly in common between the two independent studies. Eleven of the 18 genera became significantly more abundant and 7 genera became significantly less abundant after WD-feeding for two weeks. **b**, Heatmap showing the fold change of each of the 18 genera identified in panel (**a**)

that differed in both independent *in vivo* studies. **c**, Plot of the abundance changes for the 18 genera identified in panel (**a**) for WD-feeding relative to CHD-feeding (red indicates more abundant in WD-fed animals and blue indicates less abundant in WD-fed animals). **d**, A heat map showing how oral peptide treatment affected the abundance of the 18 genera identified in panel (**a**). The negative correlation for c[wLwReQeR] against the bacteria that became more abundant in WD-feeding indicates that c[wLwReQeR] remodeled the gut microbiome by causing those genera to become less abundant. In contrast, c[wLwKhShK] treatment promoted the growth of the bacterial genera that became less abundant with WD-feeding, as indicated the positive correlation for c[wLwKhShK] against WD-less abundant genera. All microbiota samples in this figure were taken from 2-wk feces samples of LDLr$^{-/-}$ mice.
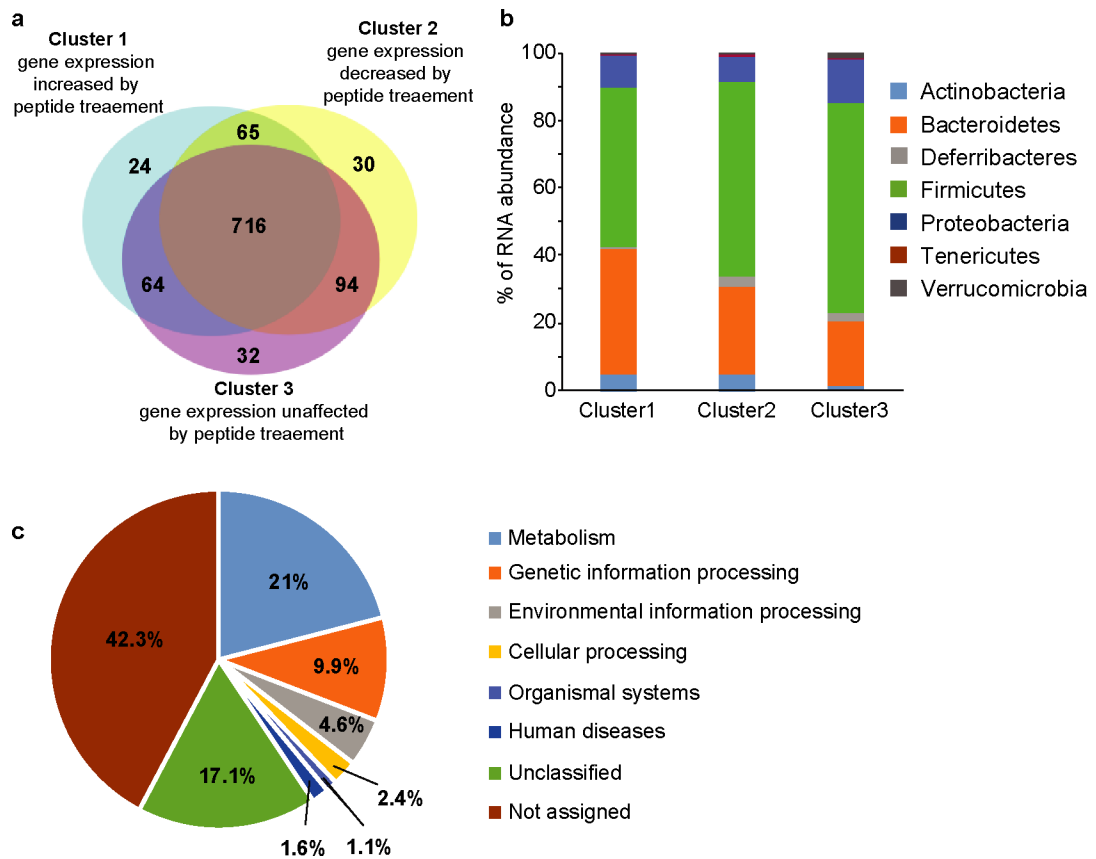
Extended Data Fig. 9. Cyclic peptide c[wLwReQeR] altered the gut microbiota transcriptome without drastically affecting the gut microbiota composition.

a, Peptide-mediated changes in gene expression could be grouped into three main clusters. Cluster 1 and Cluster 2 contained bacterial genes for which expression was increased or decreased, respectively, by peptide treatment. Cluster 3 contained genes that were altered by the WD compared the CHD, but not affected by peptide treatment. The Venn diagram reports the number of bacterial species having transcripts within each cluster. The majority of species had transcripts within each cluster, indicative of broad transcriptomic changes across the gut microbiome. **b**, Gene expression levels from each bacterial phylum for the three gene expression Clusters. RNA expression was increased from Bacteroidetes and decreased from Firmicutes in Cluster 1 compared to Cluster 2 or Cluster 3. **c**, Bacterial

functions of the gut microbiome, as predicted by transcriptome analysis of feces samples from CHD fed mice. The values shown are the percentage of reads from the transcriptome analysis belonging to each category.
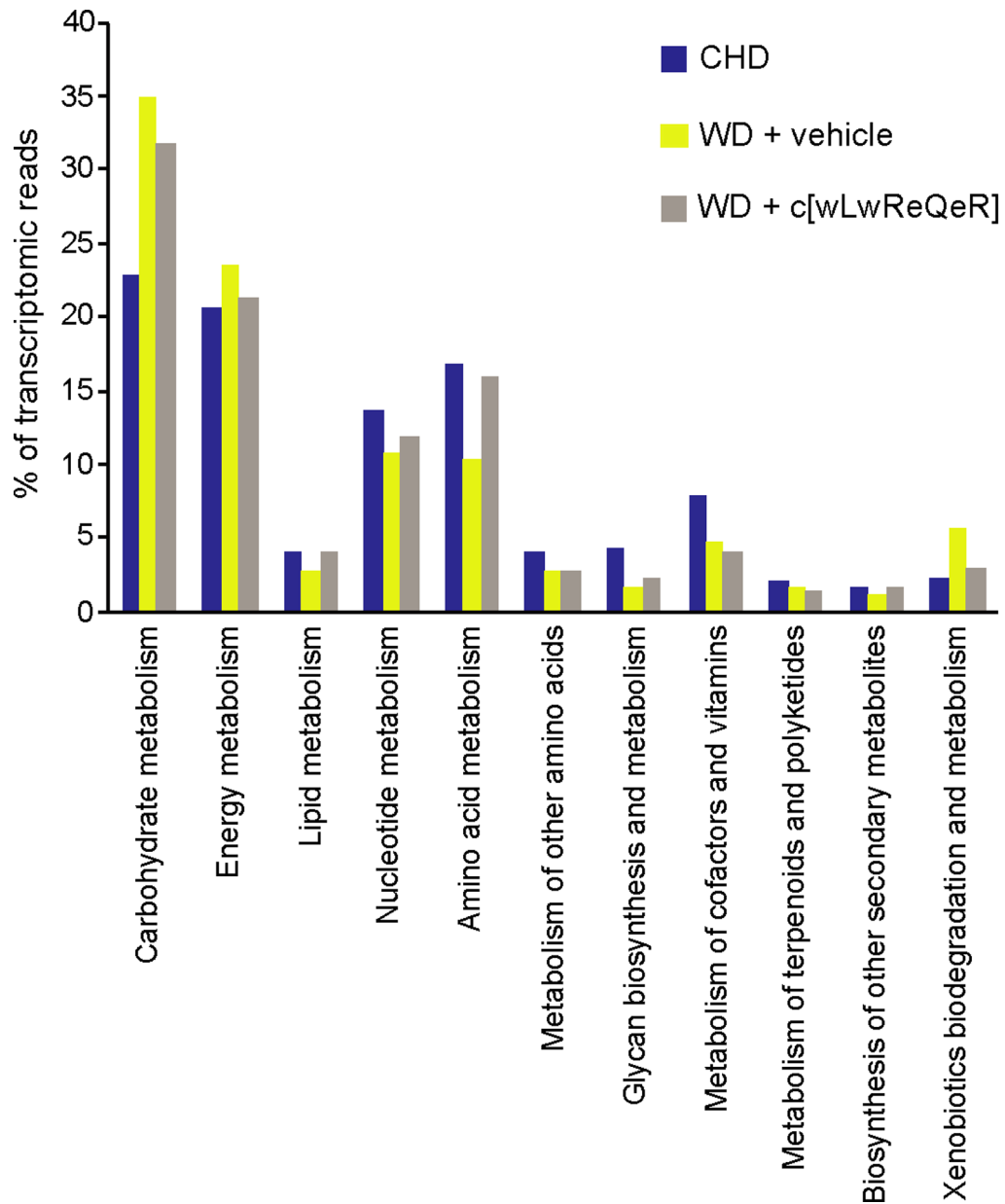
Extended Data Fig. 10. Comparison of gut microbiome gene expression levels for metabolic processes among the different treatment groups.

The graph shows gene expression levels of various metabolic processes for the CHD, WD, or c[wLwReQeR]-treated animals, as determined by RNA-Seq analysis of fecal samples taken after a 2-wk treatment period.

Supplementary Material

Refer to Web version on PubMed Central for supplementary material.

Acknowledgements

REFERENCES

1. Lozupone CA, Stombaugh JI, Gordon JI, Jansson JK & Knight R Diversity, stability and resilience of the human gut microbiota. Nature 489, 220–230 (2012). [PubMed: 22972295]

2. Cho I & Blaser MJ The human microbiome: At the interface of health and disease. Nat. Rev. Genet 13, 260–270 (2012). [PubMed: 22411464]

3. Brown JM & Hazen SL Microbial modulation of cardiovascular disease. Nat. Rev. Microbiol 16, 171–181 (2018). [PubMed: 29307889]

4. Zhao L The gut microbiota and obesity: From correlation to causality. Nat. Rev. Microbiol 11, 639–647 (2013). [PubMed: 23912213]

5. Maruvada P, Leone V, Kaplan LM & Chang EB The human microbiome and obesity: Moving beyond associations. Cell Host Microbe 22, 589–599 (2017). [PubMed: 29120742]

6. Khan MT, Nieuwdorp M & Baeckhed F Microbial modulation of insulin sensitivity. Cell Metab. 20, 753–760 (2014). [PubMed: 25176147]

7. Pedersen HK et al. Human gut microbes impact host serum metabolome and insulin sensitivity. Nature 535, 376–381 (2016). [PubMed: 27409811]

8. Sharon G, Sampson TR, Geschwind DH & Mazmanian SK The central nervous system and the gut microbiome. Cell 167, 915–932 (2016). [PubMed: 27814521]

9. Turnbaugh PJ et al. The effect of diet on the human gut microbiome: A metagenomic analysis in humanized gnotobiotic mice. Sci. Transl. Med 1, 6ra14–16ra14 (2009).

10. Kau AL, Ahern PP, Griffin NW, Goodman AL & Gordon JI Human nutrition, the gut microbiome and the immune system. Nature 474, 327–336 (2011). [PubMed: 21677749]

11. Carmody RN et al. Diet dominates host genotype in shaping the murine gut microbiota. Cell Host Microbe 17, 72–84 (2015). [PubMed: 25532804]

12. Furusawa Y et al. Commensal microbe-derived butyrate induces the differentiation of colonic regulatory T cells. Nature 504, 446–450 (2013). [PubMed: 24226770]

13. Rios-Covian D et al. Intestinal short chain fatty acids and their link with diet and human health. Front. Microbiol 7, 185 (2016). [PubMed: 26925050]

14. Perry RJ et al. Acetate mediates a microbiome-brain-β-cell axis to promote metabolic syndrome. Nature 534, 213–217 (2016). [PubMed: 27279214]

15. Hsiao EY et al. Microbiota modulate behavioral and physiological abnormalities associated with neurodevelopmental disorders. Cell 155, 1451–1463 (2013). [PubMed: 24315484]

16. Dodd D et al. A gut bacterial pathway metabolizes aromatic amino acids into nine circulating metabolites. Nature 551, 648–652 (2017). [PubMed: 29168502]

17. de Aguiar Vallim TQ, Tarling EJ & Edwards PA Pleiotropic roles of bile acids in metabolism. Cell Metab. 17, 657–669 (2013). [PubMed: 23602448]

18. Wahlstroem A, Sayin SI, Marschall H-U & Baeckhed F Intestinal crosstalk between bile acids and microbiota and its impact on host metabolism. Cell Metab. 24, 41–50 (2016). [PubMed: 27320064]

19. Jia W, Xie G & Jia W Bile acid-microbiota crosstalk in gastrointestinal inflammation and carcinogenesis. Nat. Rev. Gastroenterol. Hepatol 15, 111–128 (2018). [PubMed: 29018272]

20. Schmidt TSB, Raes J & Bork P The human gut microbiome: From association to modulation. Cell 172, 1198–1215 (2018). [PubMed: 29522742]

21. Wang Z et al. Non-lethal inhibition of gut microbial trimethylamine production for the treatment of atherosclerosis. Cell 163, 1585–1595 (2015). [PubMed: 26687352]

22. Zhu W et al. Precision editing of the gut microbiota ameliorates colitis. Nature 553, 208–211 (2018). [PubMed: 29323293]

23. Li F et al. Microbiome remodelling leads to inhibition of intestinal Farnesoid X receptor signalling and decreased obesity. Nat. Commun 4, 2384 (2013). [PubMed: 24064762]

24. Sanders ME, Merenstein DJ, Reid G, Gibson GR & Rastall RA Probiotics and prebiotics in intestinal health and disease: From biology to the clinic. Nat. Rev. Gastroenterol. Hepatol 16, 605–616 (2019). [PubMed: 31296969]

25. Shepherd ES, DeLoache WC, Pruss KM, Whitaker WR & Sonnenburg JL An exclusive metabolic niche enables strain engraftment in the gut microbiota. Nature 557, 434–438 (2018). [PubMed: 29743671]

26. Chen M-L et al. Resveratrol attenuates trimethylamine-N-oxide (TMAO)-induced atherosclerosis by regulating TMAO synthesis and bile acid metabolism via remodeling of the gut microbiota. MBio 7, e02210–02215 (2016). [PubMed: 27048804]

27. Maier L et al. Extensive impact of non-antibiotic drugs on human gut bacteria. Nature 555, 623–628 (2018). [PubMed: 29555994]

28. De Santis P, Morosetti S & Rizzo R Conformational analysis of regular enantiomeric sequences. Macromolecules 7, 52–58 (1974). [PubMed: 4837982]

29. Pavone V et al. Regularly alternating L,D-peptides. III. Hexacyclic peptides from valine or phenylalanine. Biopolymers 28, 215–223 (1989). [PubMed: 2720106]

30. Ghadiri MR, Granja JR, Milligan RA, McRee DE & Khazanovich N Self-assembling organic nanotubes based on a cyclic peptide architecture. Nature 366, 324–327 (1993). [PubMed: 8247126]

31. Fernandez-Lopez S et al. Antibacterial agents based on the cyclic D,L-alpha-peptide architecture. Nature 412, 452–456 (2001). [PubMed: 11473322]

32. Dartois V et al. Systemic antibacterial activity of novel synthetic cyclic peptides. Antimicrob. Agents Chemother 49, 3302–3310 (2005). [PubMed: 16048940]

33. Fletcher JT, Finlay JA, Callow ME, Callow JA & Ghadiri MR A combinatorial approach to the discovery of biocidal six-residue cyclic D,L-alpha-peptides against the bacteria methicillin-resistant Staphylococcus aureus (MRSA) and E. coli and the biofouling algae Ulva linza and Navicula perminuta. Chem. Eur. J 13, 4008–4013 (2007). [PubMed: 17304598]

34. Ley RE, Turnbaugh PJ, Klein S & Gordon JI Microbial ecology: Human gut microbes associated with obesity. Nature 444, 1022–1023 (2006). [PubMed: 17183309]

35. Martinez KB, Leone V & Chang EB Western diets, gut dysbiosis, and metabolic diseases: Are they linked? Gut Microbes 8, 130–142 (2017). [PubMed: 28059614]

36. Sonnenburg ED et al. Diet-induced extinctions in the gut microbiota compound over generations. Nature 529, 212–215 (2016). [PubMed: 26762459]

37. Koh A, De Vadder F, Kovatcheva-Datchary P & Baeckhed F From dietary fiber to host physiology: Short-chain fatty acids as key bacterial metabolites. Cell 165, 1332–1345 (2016). [PubMed: 27259147]

38. Clark TD et al. Cylindrical beta-sheet peptide assemblies. J. Am. Chem. Soc 120, 8949–8962 (1998).

39. Kennedy EA, Baldridge MT & King KY Mouse microbiota models: Comparing germ-free mice and antibiotics treatment as tools for modifying gut bacteria. Front. Physiol 9, 1534 (2018). [PubMed: 30429801]

40. Lundberg R et al. Antibiotic-treated versus germ-free rodents for microbiota transplantation studies. Gut Microbes 7, 68–74 (2016). [PubMed: 26744774]

41. Zarrinpar A et al. Antibiotic-induced microbiome depletion alters metabolic homeostasis by affecting gut signaling and colonic metabolism. Nat. Commun 9, 2872 (2018). [PubMed: 30030441]

42. Miyake JH et al. Transgenic expression of cholesterol-7-alpha-hydroxylase prevents atherosclerosis in C57BL/6J mice. Arterioscler. Thromb. Vasc. Biol 22, 121–126 (2002). [PubMed: 11788471]

43. Li T & Chiang JYL Bile acid signaling in metabolic disease and drug therapy. Pharmacol. Rev 66, 948–983 (2014). [PubMed: 25073467]

44. Zhang Y et al. FXR deficiency causes reduced atherosclerosis in LDLr–/– mice. Arterioscler. Thromb. Vasc. Biol 26, 2316–2321 (2006). [PubMed: 16825595]

45. Sayin SI et al. Gut microbiota regulates bile acid metabolism by reducing the levels of tauro-beta-muricholic acid, a naturally occurring FXR antagonist. Cell Metab. 17, 225–235 (2013). [PubMed: 23395169]

46. Ridker PM et al. Antiinflammatory therapy with canakinumab for atherosclerotic disease. N. Engl. J. Med 377, 1119–1131 (2017). [PubMed: 28845751]

47. Ross R Atherosclerosis--an inflammatory disease. N. Engl. J. Med 340, 115–126 (1999). [PubMed: 9887164]

48. Mazmanian SK, Round JL & Kasper DL A microbial symbiosis factor prevents intestinal inflammatory disease. Nature 453, 620–625 (2008). [PubMed: 18509436]

49. Caesar R, Fak F & Backhed F Effects of gut microbiota on obesity and atherosclerosis via modulation of inflammation and lipid metabolism. J. Intern. Med 268, 320–328 (2010). [PubMed: 21050286]

50. Piccirillo CA, d'Hennezel E, Sgouroudis E & Yurchenko E CD4+FOXP3+ regulatory T cells in the control of autoimmunity: In vivo veritas. Curr. Opin. Immunol 20, 655–662 (2008). [PubMed: 18926906]

51. Ait-Oufella H et al. Natural regulatory T cells control the development of atherosclerosis in mice. Nat. Med 12, 178–180 (2006). [PubMed: 16462800]

52. Schiering C et al. The alarmin IL-33 promotes regulatory T-cell function in the intestine. Nature 513, 564–568 (2014). [PubMed: 25043027]

53. Round JL & Mazmanian SK Inducible FOXP3+ regulatory T-cell development by a commensal bacterium of the intestinal microbiota. Proc. Natl. Acad. Sci. U.S.A 107, 12204–12209 (2010). [PubMed: 20566854]

54. Sefik E et al. Individual intestinal symbionts induce a distinct population of RORγ+ regulatory T cells. Science 349, 993–997 (2015). [PubMed: 26272906]

55. Soroosh P et al. Oxysterols are agonist ligands of RORγt and drive Th17 cell differentiation. Proc. Natl. Acad. Sci. U.S.A 111, 12163–12168 (2014). [PubMed: 25092323]

56. Freigang S et al. Fatty acid-induced mitochondrial uncoupling elicits inflammasome-independent IL-1α and sterile vascular inflammation in atherosclerosis. Nat. Immunol 14, 1045–1053 (2013). [PubMed: 23995233]

57. Schloss PD et al. Introducing MOTHUR: Open-source, platform-independent, community-supported software for describing and comparing microbial communities. Appl. Environ. Microbiol 75, 7537–7541 (2009). [PubMed: 19801464]

58. Love MI, Huber W & Anders S Moderated estimation of fold change and dispersion for RNA-Seq data with DESeq2. Genome Biol. 15, 550 (2014). [PubMed: 25516281]

59. Staley C et al. Stable engraftment of human microbiota into mice with a single oral gavage following antibiotic conditioning. Microbiome 5, 87 (2017). [PubMed: 28760163]

60. Matranga Christian B et al. Enhanced methods for unbiased deep sequencing of Lassa and Ebola RNA viruses from clinical and biological samples. Genome Biol. 15, 519 (2014). [PubMed: 25403361]

61. Li H & Durbin R Fast and accurate short read alignment with Burrows-Wheeler transform. Bioinformatics 25, 1754–1760 (2009). [PubMed: 19451168]

62. Anders S, Pyl PT & Huber W HTSeq--a Python framework to work with high-throughput sequencing data. Bioinformatics 31, 166–169 (2015). [PubMed: 25260700]

63. Anders S & Huber W Differential expression analysis for sequence count data. Genome Biol. 11, R106 (2010). [PubMed: 20979621]

64. Buchfink B, Xie C & Huson DH Fast and sensitive protein alignment using DIAMOND. Nat. Methods 12, 59–60 (2015). [PubMed: 25402007]

65. O'Leary NA et al. Reference sequence (REFSeq) database at NCBI: Current status, taxonomic expansion, and functional annotation. Nucleic Acids Res. 44, D733–745 (2016). [PubMed: 26553804]

66. Huson DH et al. MEGAN community edition - interactive exploration and analysis of large-scale microbiome sequencing data. PLoS Comput. Biol 12, e1004957 (2016). [PubMed: 27327495]

67. Hainer Sarah J et al. Suppression of pervasive noncoding transcription in embryonic stem cells by ESBAF. Genes Dev. 29, 362–378 (2015). [PubMed: 25691467]

68. Li B & Dewey CN RSEM: Accurate transcript quantification from RNA-Seq data with or without a reference genome. BMC Bioinformatics 12, 323 (2011). [PubMed: 21816040]

69. Huang da W, Sherman BT & Lempicki RA Systematic and integrative analysis of large gene lists using DAVID bioinformatics resources. Nat. Protoc 4, 44–57 (2009). [PubMed: 19131956]

70. Huang DW, Sherman BT & Lempicki RA Bioinformatics enrichment tools: Paths toward the comprehensive functional analysis of large gene lists. Nucleic Acids Res. 37, 1–13 (2009). [PubMed: 19033363]

Author Manuscript

Author Manuscript

Author Manuscript

Author Manuscript
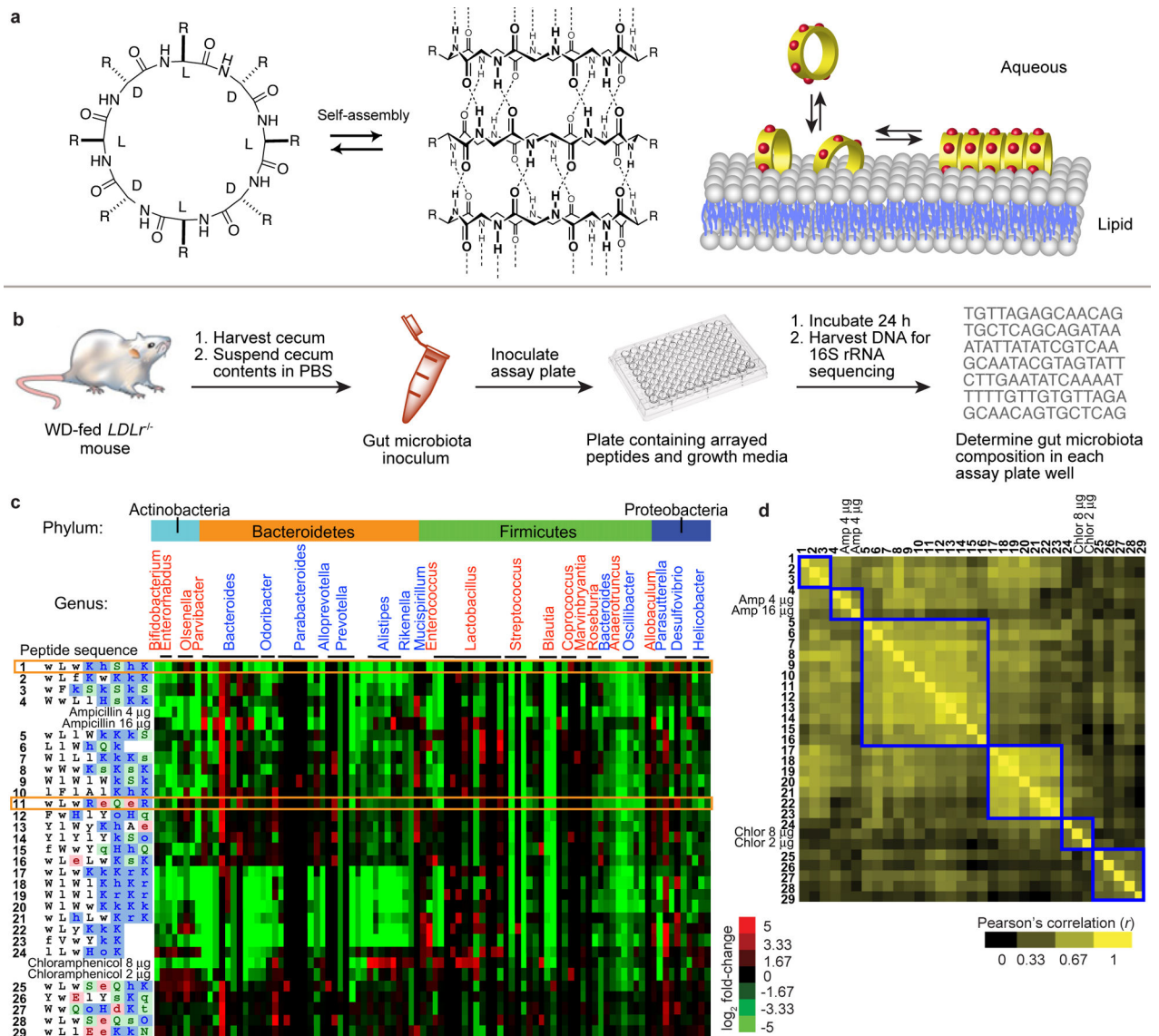
**Figure 1. Cyclic D,L-α-peptides modulate gut microbiota *in vitro*.**
a, Schematic illustration of cyclic D,L-α-peptide structure and hydrogen bond-directed self-assembly in a lipid/cell membrane environment. **b**, Schematic overview of the *in vitro* screening approach and bioinformatics analysis. Cecum harvest and all assay steps were performed under anaerobic conditions. **c**, Genus level changes in bacterial abundance caused by cyclic peptide treatment (64 μM), relative to an untreated control, as determined by 16S rRNA sequencing. Peptide sequences are shown on the left with L-amino acids as upper-case letters, D-amino acids as lower-case letters, cationic residues shaded blue, anionic residues in red, polar neutral residues in green, and hydrophobic residues not shaded. Peptides are ordered by hierarchical clustering such that sequences producing similar remodeling effects on the microbiota composition are clustered near each other. The genus and phylum level categorizations are shown at the top. Genus level names are colored red or blue for Gram-positive or Gram-negative bacteria, respectively. Peptides **1** and **11**, highlighted with blue boxes, were chosen for further *in vivo* testing. **d**, Heatmap showing

pairwise comparison of different peptides (64 μM) in remodeling gut microbiota. Higher correlation indicates that those peptides show more similar effects in changing the microbiota composition. The blue squares highlight six peptide sequence clusters, each affecting the microbiota differently.
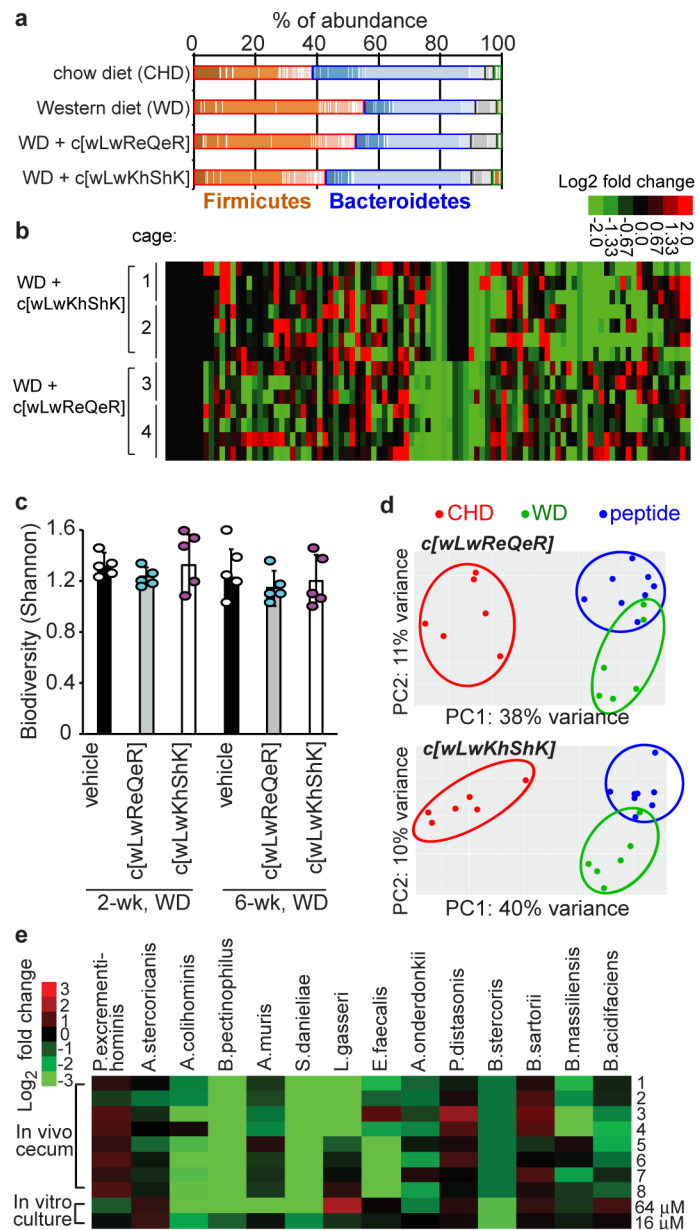
Figure 2. Cyclic D,L-α-peptide-induced *in vivo* remodeling of LDLr$^{-/-}$ mouse gut microbiota.
Three groups of WD-fed mice were treated with either vehicle or ~35 mg/kg daily oral
dosing of the peptides shown for 10 weeks. A fourth group of mice was fed a standard, low-
fat CHD with no treatment. **a**, Stacked bar graph showing the abundance of each bacterial
genus in feces at 2 weeks. Bacteria belonging to the two main phyla, Firmicutes and
Bacteroidetes, are labeled. n=5 animals per group. **b**, Heatmap showing the fold-change of
bacterial species (n=97) within genera that were significantly affected (adjusted p-value <
0.1 as determined by DESeq2 using a two-sided Wald test with adjustment for multiple
comparisons using the Benjamini-Hochberg method) by peptide treatment relative to vehicle
controls. Fecal samples were obtained from mice after oral dosing of the peptides for a 2-wk
period (n=7 animals for c[wLwReQeR] and c[wLwKhShK] groups; n=8 animals for WD

vehicle group). **c**, Peptide induced remodeling did not affect the biodiversity of the gut microbiome after 2-wk or 6-wk treatment (n=5 animals per group, fecal samples). Data are shown as mean ± SD. **d**, Principal-component analysis of genera abundance of WD animals with peptide treatment, WD/vehicle and CHD/vehicle (n=8 animals for c[wLwReQeR] and c[wLwKhShK] groups; n=6 animals for CHD and WD groups; data shown for 2-wk timepoint). **e**, Changes in microbiota abundance mediated by peptide c[wLwReQeR] were generally similar for the *in vitro* screen and *in vivo* treatment (n=8 animals for *in vivo* group; n=2 independent samples from *in vitro* group). The species shown are those for which peptide treatment *in vivo* caused a significantly different abundance compared to vehicle group (adjusted *p*-value < 0.05 as determined by DESeq2 using a two-sided Wald test with adjustment for multiple comparisons using the Benjamini-Hochberg method). *In vivo* data is for the 2-wk timepoint.
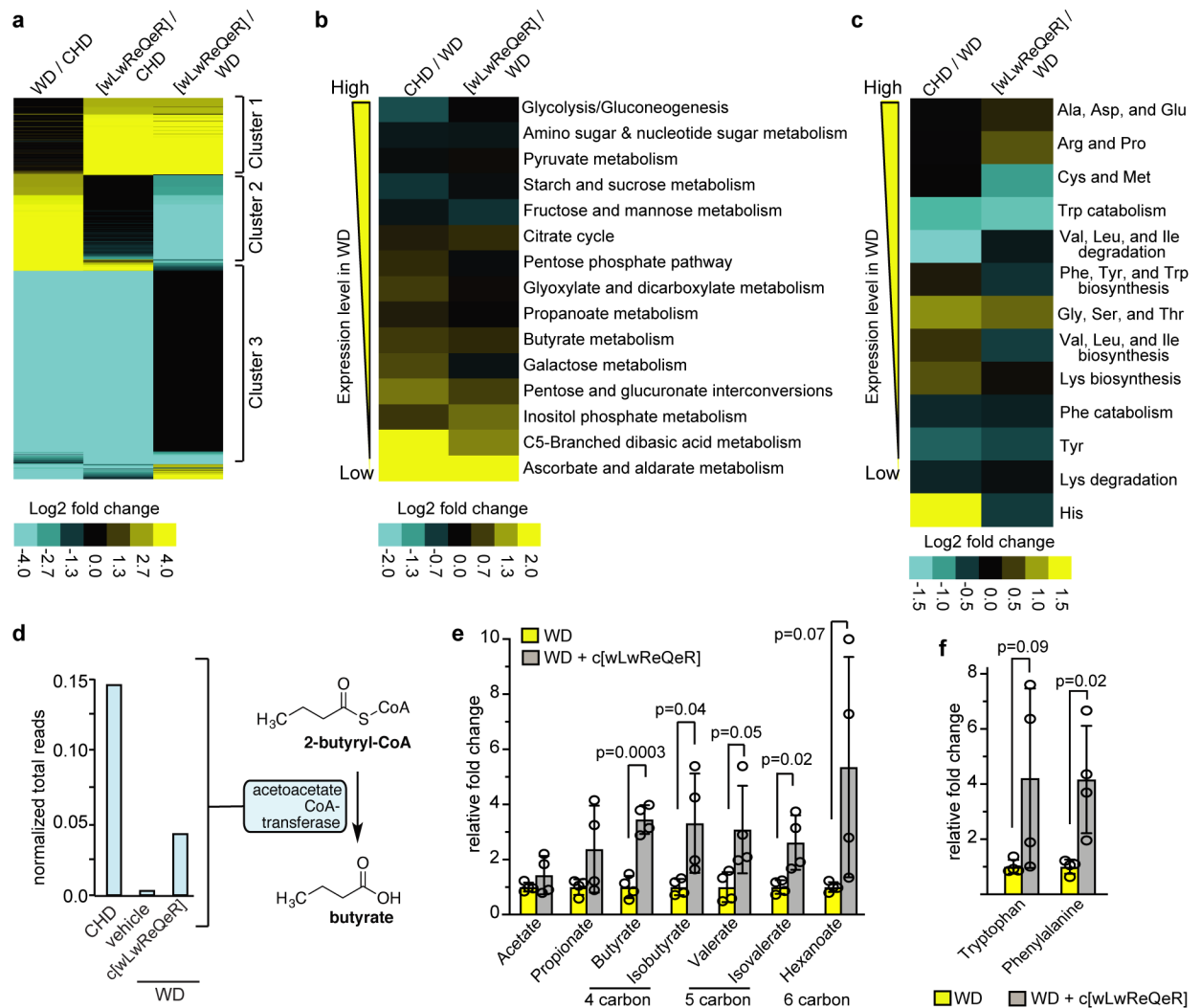
Figure 3. Peptide treatment of WD-fed mice induced metabolic changes and transcriptional reprogramming of the gut microbiota.

a, RNA-Seq analysis of bacterial RNA from feces following a 2-wk treatment period. The heatmap shows differences in expression (unsupervised hierarchical clustering of genes misregulated) between the indicated groups for every identified gene. The expression changes can be grouped into three main clusters. Clusters 1 and 2 contain bacterial genes for which expression was generally increased or decreased, respectively, by peptide treatment. Cluster 3 contains genes that were altered by the WD, but not affected by peptide (bracket location). **b**, An example of functional metagenomics pathway analysis is shown for carbohydrate metabolism. RNA-sequence reads were mapped to a reference genome and assigned a function, and the aggregate expression level changes for sequences within a given function group were plotted. Among other predicted changes, butyrate metabolism was increased by peptide treatment. **c**, The change in gene expression level of various amino acid-related metabolisms from CHD or peptide treatment animals compared to WD. The heatmap is sorted by gene expression level of each metabolism category in WD. **d**, Functional metagenomics analyses indicated changes to enzyme expression levels involved in butyrate biosynthesis. Peptide treatment remodeled gut bacteria metagenomics to increase

acetoacetate-CoA transferase levels, which would lead to higher levels of butyrate. **e**, SCFA levels in feces after 2-wk treatment, as determined by mass spectrometry. Butyrate was increased by 4-fold in treated mice (n=4 animals per group). **f**, Relative change in fecal concentrations of aromatic amino acids after 2-wk peptide treatment (n=4 animals per group). In the graphs, values are shown as mean ± SD, and *p* values were determined by two-tailed Student's t-test.
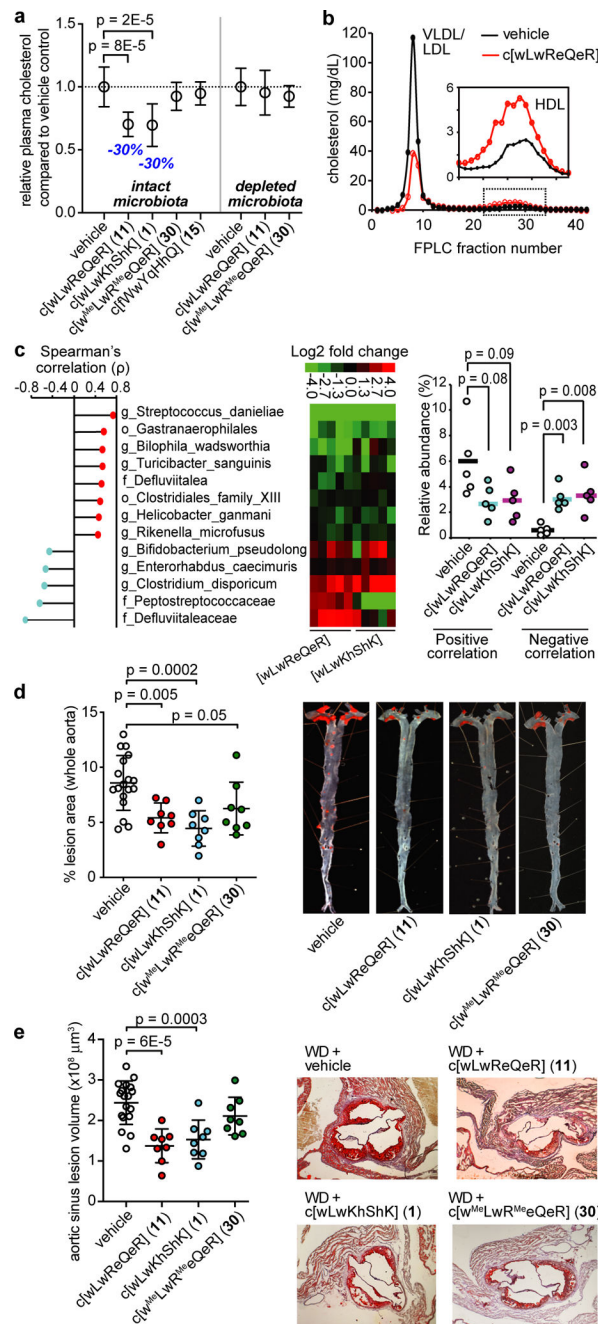
Figure 4. Peptide treatment reduced the development of atherosclerosis in WD-fed LDLr⁻/⁻ mice.

a, Comparison of peptide effects on plasma cholesterol levels from experiments with intact or antibiotic-depleted gut microbiota. Peptides **11** and **1** (~35 mg/kg daily oral dosing for 2-wk) reduced plasma total cholesterol in WD-fed *LDLr⁻/⁻* mice with intact microbiota compared to the WD-fed vehicle group (n=8 animals for peptide **1**, **11**, and **30** groups; n=9 animals for peptide **15** group; n=18 animals for vehicle group). Microbiota depletion blocked the cholesterol-lowering effect of **11**, supporting that the mechanism of action involves direct targeting and remodeling of the gut microbiota by the peptides (n=5 animals

for each depleted microbiota group). Data are shown as mean ± SD and adjusted *p*-values were determined by one-way ANOVA with post-hoc Dunnett test. **b**, Plasma from fasted mice (pooled from n=8 animals per group) from the 2-wk time point was fractionated by gel filtration, showing that peptide treatment reduced VLDL and LDL levels, and increased HDL levels. **c**, A number of bacterial taxa were positively or negatively associated with 2-wk plasma cholesterol levels (n=5 animals for each group). The graph on the left shows correlation values for each taxon. In the middle, the heatmap shows how the abundance of each taxon was affected by the peptides relative to vehicle *in vivo*. Notably, the bacteria positively correlated with plasma cholesterol levels were generally reduced in abundance by the peptides, and vice versa. On the right, the change in summed abundance of the positively or negatively correlated OTUs are shown. The *p*-values were determined by two-tailed Student's t-test. **d**, 10-wk peptide treatment (n=8 animals per group) reduced the development of atherosclerotic lesions compared to vehicle controls (n=18 animals), as determined by *en face* staining of the aorta. A representative image of a stained aorta (lesions stain as red) is shown for each group. In panels **d**-**e**, data are shown as mean ± SD and adjusted *p*-values were determined by one-way ANOVA with post-hoc Dunnett test. **e**, Atherosclerotic lesion volumes were reduced by peptide treatment as determined by sectioning of the aortic sinus (n=8 animals per treated group and n=18 animals in vehicle control group). A representative image is shown for each group.
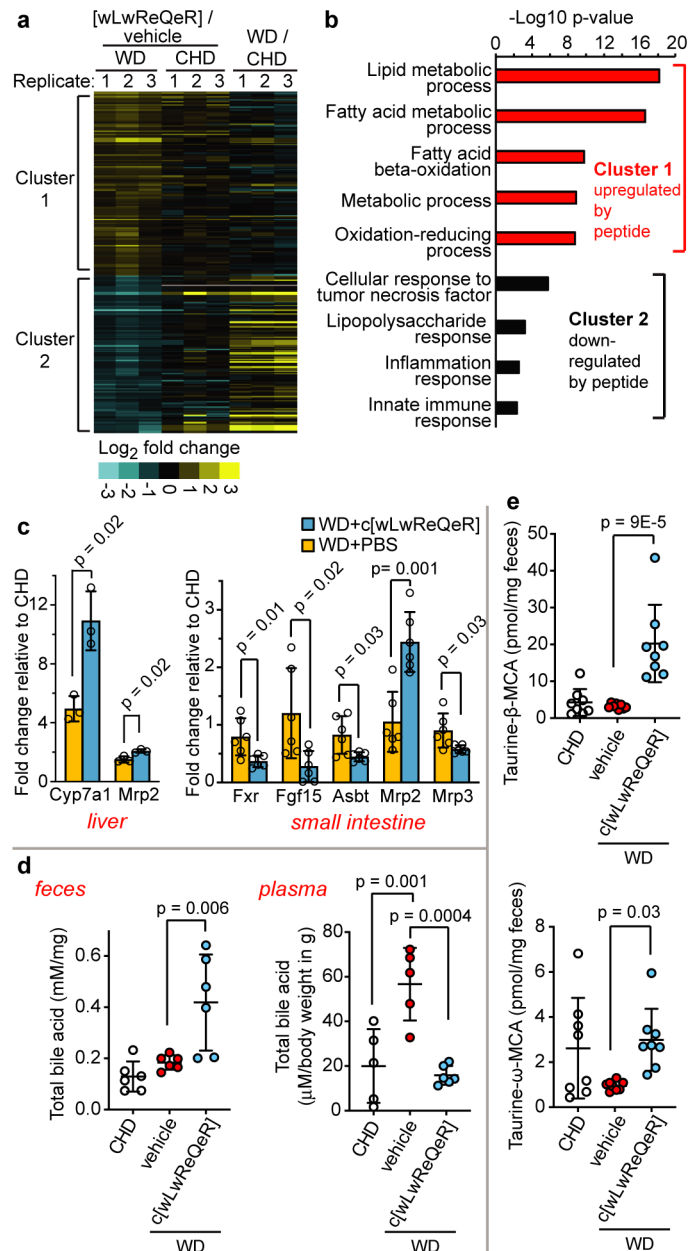
Figure 5. Peptide treatment altered gene expression and bile acid composition in WD-fed LDLr$^{-/-}$ mice.

a, Heat-map showing expression levels in genes for which there were significant differences (adjusted p-value < 0.1 as determined by DESeq2 using a two-sided Wald test with adjustment for multiple comparisons using the Benjamini-Hochberg method) between the peptide-treated WD and vehicle WD groups, as determined by RNA-Seq. Samples were from liver tissue after a 2-wk treatment period. Four total groups of animals were analyzed: two WD and two CHD groups treated either with peptide or vehicle (n=3 animals per group). The altered genes were grouped into two clusters for which peptide treatment cause increases (Cluster 1) or decreases (Cluster 2) in expression level. **b**, Gene ontology analysis for significantly changed genes in liver tissue. **c**, mRNA expression levels of several genes

involved in sterol/bile acid metabolism, as determined by quantitative PCR of samples from liver (n=3 animals per group) and small intestine (n=5 animals per group). Values are shown as mean ± SD, and p-values were determined by two-tailed Student's t-test. **d**, Total bile acid levels in the feces (n=6 animals per group) or plasma (n=5 animals for CHD and WD vehicle groups; n=6 animals for c[wLwReQeR] group) of CHD, WD vehicle, or peptide-treated animals, as determined by enzymatic bile acid assay. The data are shown as mean ± SD and adjusted p-values were determined by one-way ANOVA with post-hoc Dunnett test. **e**, The level of taurine conjugated muricholic acids in feces from CHD, WD, or peptide-treated animals (n=8 animals per group), as determined by targeted metabolomics. The data are shown as mean ± SD and adjusted p-values were determined by one-way ANOVA with post-hoc Dunnett test.
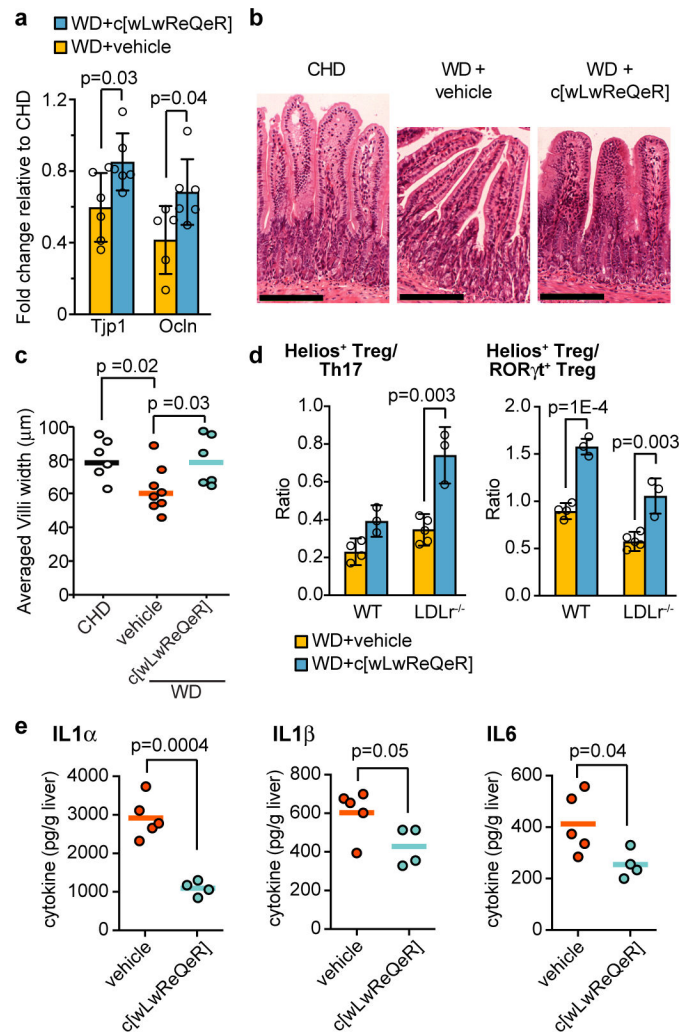
Figure 6. Peptide treatment reduced WD-induced inflammation in LDLr$^{-/-}$ mice via several gut microbiota-dependent mechanisms.

a, Expression of tight junction markers Tjp1 and Ocln in small intestine of vehicle- or peptide-treated WD-fed animals, as determined by qRT-PCR (n=3 animals per group). In all panels, the data are shown as the mean ± SD and *p*-values were determined by two-tailed Student's t-test. **b,c** Representative images of ileum sections and average villi width showing the recovery in intestinal villi width after cyclic peptide treatment (scale bars, 300 μm). Villi width was determined from 23, 44, and 34 individual illeum sections taken from n=6, 8, and 6 animals for the CHD, WD + vehicle, and WD + peptide groups, respectively. **d**, Composition of regulatory T cell population in lamina propria from vehicle or peptide treated animals, as indicated by the ratio of Helios$^+$ Treg cells to Th17 cells and RORγt$^+$ Treg cells in wild type (WT) or *LDLr*$^{-/-}$ mice (n=3 mice each for peptide-treated WT and LDLr$^{-/-}$ groups; n=4 animals for vehicle-treated WT group; n=5 animals for vehicle-treated LDLr$^{-/-}$ group). **e**, Peptide treatment reduced the levels of certain hepatic cytokines/chemokines, as indicated by luminex analysis (n=5 animals for vehicle group; n=4 animals for c[wLwReQeR] group).